

## Effect of Maceral Composition and Vitrinite Reflectance on the Combustion Behavior of Six hvA Bituminous Coals

Sung-Tae Kim, Alan W. Scaroni  
and  
Mohammad Fatemi-Badi

The Pennsylvania State University  
Combustion Laboratory  
405 Academic Activities Building  
University Park, PA 16802

### Introduction

A common way of classifying coals is by rank, that is, according to the degree of metamorphism, or progressive alteration of the plant debris as it is transformed into the natural series from lignite to anthracite. In the United States the rank classification system was established by the American Society for Testing and Materials (ASTM), and is based on the percent volatile matter and fixed carbon obtained from the proximate analysis and on a dry, mineral-matter-free basis, and the heating value in British thermal units per pound (Btu/lb) expressed on a moist, mineral-matter-free basis.<sup>(1)</sup> Each rank of coal from lignite to anthracite has distinctive chemical and physical characteristics which influence the behavior in a given application. This rank classification is commonly used as a guide in the selection of pulverized coal for use in utility and industrial boilers. Although rank can indicate, in some cases, general processing behavior, it is not sufficient to characterize the specific behavior of a coal under specific utilization conditions. This derives, at least in part, from the fact that different maceral compositions for coals of the same rank can give rise to different properties, and hence, different behavior during processing. Therefore, assessment or prediction of processing, particularly combustion, behavior based on rank alone is not reliable. In higher rank coals, however, where the differences between macerals is less significant,<sup>(2)</sup> the behavioral differences as a consequence of maceral composition are less significant.

Due to the relatively high vitrinite concentration in American coals, their chemical analyses tend to reflect the composition and properties of the vitrinite. Therefore, the parameters used to classify coals according to rank often reflect the rank of the vitrinite. Further, the characteristics of vitrinite are considered to change in a fairly uniform manner throughout the coalification series. One characteristic of vitrinite which can be measured easily is its reflectance. It is a measure of percent light reflected from a polished surface of coal. Because the degree of petrographic heterogeneity is much greater in lignites than in coals of higher rank, there are some difficulties in determination of vitrinite reflectance in these coals.

It has been observed in practice that a switch from a familiar coal can lead to a change in the amount of unburnt carbon in the fly ash from a utility boiler. There are many possible explanations for this, but in recent years increasing attention is being focussed upon the maceral composition of coals as being a contributor to the problem. From the available published work, relationships between certain petrographic properties and coal combustion behavior can be inferred. In particular, inertinite macerals appear to burn less readily than the so-called "reactive macerals".<sup>(3,4)</sup> Thus, coals with high inertinite contents may require high temperature and/or long residence time to avoid high unburnt carbon loss. This is supported by results from laboratory experiments and some industrial experience.<sup>(3-8)</sup> The purpose of the current work was to determine the effect of maceral composition and vitrinite reflectance on the combustion behavior of six maceral-rich hvA bituminous coals.

## Experimental

Combustion experiments were conducted in an entrained-flow reactor, a schematic diagram of which is given in Figure 1. The system is composed of a preheater, water-cooled feed probe, cyclone, water-cooled collector probe and char collector. A stream of coal particles was fed by the screw feeder and entrained in a primary gas stream at ambient temperature, then passed through a water-cooled probe and injected at the top of a hot cylindrical reaction chamber, which was maintained electrically at a specified reaction temperature. At the same time, a secondary and larger stream of carrier gas, which was preheated to the reactor temperature, was isokinetically injected around the primary gas stream in laminar flow to ensure that the particles were not dispersed radially to the furnace walls. A ceramic disk was placed above the injector tip to serve as a flow straightener. The secondary gas temperature was adjusted so that upon mixing of the primary and secondary gases the combined gas stream attained the desired reaction temperature. Heating elements around the reactor produced a uniform wall temperature. The estimated heating rate of the particles is  $10^3$  to  $10^4$  K/sec. The entrained coal particles travelled in a pencil-like stream down the axis of the reactor. The products of combustion were collected through a water-cooled collector probe that quenched reactions. Solid products (chars) were collected in the cyclone, condensable liquids (tars) were deposited on the filter, and gaseous products were released into an exhaust stack. Detailed design specifications and description of the ancillary equipment are presented elsewhere.<sup>(9-11)</sup>

In this study, six maceral-rich hvA bituminous coal samples were selected from the D.O.E/Penn State Coal Sample Bank. The selection was based primarily on differences in maceral composition and vitrinite reflectance. The coals were divided into two groups: one group of three having similar maceral composition but different vitrinite reflectance, and the other group having similar vitrinite reflectance but different maceral composition. Full analyses of the six samples are shown in Table 1. By way of example PSOC-1501 is referred to as a low-reflectance, vitrinite-rich coal and PSOC-1374 as a high-reflectance, vitrinite-rich coal of the same rank. A similar relationship holds for PSOC-296 and PSOC-733 (liptinite-rich coals), and PSOC-861 and PSOC-736 (inertinite-rich coals). Three particle size fractions of the six coals, with mean particle diameters of 63, 90, and 127  $\mu\text{m}$ , were prepared and used in this study.

The samples were partially combusted in the reactor at temperatures of 1073 and 1273 K and residence times of typically less than 0.3s. Coal particle residence times in the furnace were determined using a computer flow model. The governing equations and principles of this model have been discussed elsewhere.<sup>(7,12)</sup> The isokinetic velocity was 128 cm/sec for both the primary and secondary gases. Prior to an experiment the temperature profiles in the reactor were determined using a suction pyrometer. The sample collector probe was then positioned in the reactor, and the coal feeder calibrated to deliver 0.5 g/min.

Proximate analyses of the coals and resulting char samples were obtained using a Leco MAC-400 proximate Analyzer. Weight loss due to the partial combustion was calculated by using ash as a tracer. On a dry, ash-free basis the governing equation is:

$$\Delta W = 100\% \left[ 1 - \frac{A_0(100 - A_1)}{A_1(100 - A_0)} \right]$$

where  $\Delta W$  is the calculated weight loss on a dry, ash-free basis;  $A_0$  is the proximate ash content of dry coal; and  $A_1$  is the proximate ash content of dry char. An assumption in this calculation is that mineral matter in the coal does not undergo transformations during pyrolysis which would change the quantity of ash produced upon ashing the chars.

## Results and Discussion

The terms "reactives" and "inerts" as used in the coke industry will be used throughout this work. The prediction of weight loss, according to the concentration of reactive macerals, would be as follows:

For the low vitrinite reflectance group,	PSOC-1501 > PSOC-296 > PSOC-861
For the high vitrinite reflectance group,	PSOC-1374 > PSOC-733 > PSOC-736

The two vitrinite-rich coals (PSOC-1501 and PSOC-1374) and a liptinite-rich coal (PSOC-296) would be considered as reactive coals, whereas the two inertinite-rich coals (PSOC-861 and PSOC-736) would be considered as less reactive.

The effect of residence time over the range 0.1 to 0.3s on the weight loss during combustion of 100x140 mesh particles of the low and high vitrinite reflectance coals at 1073 K is shown in Figures 2 and 3, respectively. Despite having similar volatile matter contents and ASTM rank, the figures shows that the weight loss by the reactive coals (PSOC-1501 and PSOC-1374) is much higher than those of the inertinite-rich coals (PSOC-861 and PSOC-736). The concentration of reactive macerals for PSOC-1501 and PSOC-1374 were 93.9 and 95.1% compared to 61.7 and 34.9 % for the inertinite-rich PSOC-861 and PSOC-736 coals, respectively. The lower weight loss by the inertinite-rich coals is a consequence of the more aromatic nature of the inertinites. In addition, vitrinite and liptinite contain more oxygen and hydrogen, respectively, than inertinite and are thus likely to be more reactive than inertinite.

As is shown in Table 1, PSOC-296 and PSOC-733 have considerable amounts of inert macerals, 32.4% and 29.1%, respectively. Therefore, it might be expected from the maceral compositions that the weight loss of these two coals would lie between those of the vitrinite-rich and inertinite-rich coals. This can be seen for PSOC-733 in Figure 3. However, despite the relatively high inert content of PSOC-296, both vitrinite-rich PSOC-1501 and liptinite rich PSOC-296 have similar weight losses as seen in Figure 2. Based only on the reactive maceral content, therefore, the difference in weight loss behavior is much smaller than might be expected. This indicates that, during the initial stages of combustion, the concentration of inert macerals seems to have much less influence than the liptinite content. A high liptinite concentration enhances ignition, due in part to the relatively higher hydrogen content. As the H/C atomic ratio of the coal increases, ignition of the volatiles is promoted, thereby increasing the weight loss rate. A comparison of the H/C atomic ratios of the coals shows that liptinite-rich PSOC-296 has a higher H/C atomic ratio (0.83) than vitrinite-rich PSOC-1501 (0.79), Table 1. A general trend is that the low vitrinite reflectance coals (PSOC-1501, PSOC-296, and PSOC-861) tend to have higher H/C ratios than the high vitrinite reflectance coals (PSOC-1374, PSOC-733, and PSOC-736).

The effect of residence time over the range 0.1 to 0.3s on the weight loss during combustion of 100x140 mesh particles of the low vitrinite reflectance coals at 1273 K is shown in Figure 4. A comparison with Figures 1 and 3 shows that as temperature is increased the effect of maceral composition on weight loss is decreased.

Figure 5 shows the effect of residence time on the weight loss of 140x200 mesh particles of two vitrinite-rich coals (PSOC-1501 and PSOC 1374) during combustion at 1073 K. The vitrinite reflectance values for PSOC-1501 and PSOC-1374 are 0.73 and 0.89, respectively. As can be seen the low vitrinite reflectance coal showed a higher weight loss. A similar trend was observed in Figure 6 for the inertinite-rich coals PSOC-861 and PSOC-736 with vitrinite reflectances of 0.73 and 0.95, respectively.

The effect of particle size on the weight loss during combustion at 1073 K and 0.1-0.3s residence times is shown in Figures 7 through 10. Figure 7 shows the effect of particle size on the weight loss of PSOC-733. The smaller particles experienced greater weight loss than the larger ones at all residence times. Figure 8 shows a similar trend for the inertinite-rich PSOC-736. Because these coals have a considerable concentration of inert maceral, they are not likely to swell significantly. Therefore, the initial particle size will be the effective size and the weight loss will be related to the initial size. As the data in Figures 7 and 8 indicate, physical factors such as particle size may be important in determining weight loss for the less reactive (inertinite-rich) coals.

The effect of particle size is less well defined for the reactive coals. Figures 9 and 10 show the effect of particle size on the weight loss behavior of vitrinite-rich PSOC-1501 and liptinite-rich PSOC-296 during combustion at 1073 K. The curves in Figures 9 and 10 show similar trends to those observed by Tsai.<sup>(7)</sup> In both cases, the weight loss behavior was rather insensitive to particle size. Since these coals are considered to be highly reactive, the observed results may be due to their thermoplastic properties. The degree of swelling for these reactive coals is larger than for the inertinite-rich coals and higher concentrations of reactive macerals are thought to change the thermal response of the coal. Thus, the effective particle size for the reactive coals during reaction will be greater than that of the initial particle size. Because particle size changes will affect the time-temperature history of the coal particles, which in turn controls to some extent their behavior in the reactor, the weight loss behavior will vary accordingly.

The ignition delay time is dependent on the gas temperature and particle size. At short residence times (prior to ignition), where the weight loss is due to devolatilization, smaller particles of the reactive coals show higher weight loss, Figures 9 and 10. In larger particles, on the other hand, the escape of volatiles from the coal matrix is retarded, and hence weight loss is reduced. At longer residence times (after ignition), however, the weight loss by the larger particles gradually increases, until the weight loss for all particle sizes become similar. This may be due to the influence of slip velocity on the mixing of the volatiles and the oxidant at the particle surface, or due to a more reactive char.

## Summary and Conclusions

The experimental results indicate that the six hvA bituminous coals studied displayed different behavior during combustion. This was attributed to differences in maceral composition and rank as measured by vitrinite reflectance. Vitrinite-rich and liptinite-rich coals lost more weight than inertinite-rich coals under similar experimental conditions. No significant differences in weight loss were observed between vitrinite-rich and liptinite-rich coals. A lower weight loss rate is believed to be characteristic of high inertinite contents. This is probably due to the existence of high aromaticity and strong cross linkages which exist within the inertinite macerals. For coals with similar maceral compositions, although the weight loss decreased with increasing vitrinite reflectance, there was not a direct and simple correlation between the weight loss and vitrinite reflectance.

Although some smaller particles showed higher weight loss than larger particles of the same coal under similar experimental conditions, there was not a general relationship between the weight loss and the initial particle size. While the weight loss by the less reactive coals (inertinite-rich coals) was sensitive to particle size, the weight loss by the reactive coals (vitrinite-rich coals) was independent of particle size.

In summary, for the high volatile bituminous coals, rank as measured by mean maximum vitrinite reflectance and maceral composition must be considered together with ASTM rank when predicting combustion behavior.

## References

1. Annual Book of ASTM Standards, Vol. 5.05, American Society for Testing and Materials, Philadelphia, PA, 1986.
2. Van Krevelen, D. W., Coal Science, Elsevier Publishing Co., Amsterdam, 1961.
3. Nandi, B. N., Brown, T. D. and Lee, G. K., Fuel, 56, 125-130, 1977.
4. Sanyal, A., J. Inst. Energy, 56, 92-95, 1983.
5. Shibaoka, M., Fuel, 48, 285-295, 1969.
6. Lee, G. K. and Whaley, H., J. Inst. Energy, 56, 190-197, 1983.
7. Tsai, C. Y., "An Experimental Investigation of the Initial Stages of Pulverized Bituminous Coal Combustion," Ph. D. Thesis, The Pennsylvania State University, 1985.
8. Vleeskens, J. M. and Nandi, B. N., Fuel, 65, 797-802, 1986.
9. Maloney, D. J., "Effects of Preoxidation on Rapid Pyrolysis Behavior and Resultant Char Structure of Caking Coals," Ph. D. Thesis, The Pennsylvania State University, 1983.
10. Morgan, M. E., "Role of Exchangeable Cations in the Pyrolysis of Lignites," Ph. D. Thesis, The Pennsylvania State University, University, 1983.
11. Mallin, J. R., "Pyrolysis of Lignitic and Bituminous Coals in an Entrained-Flow Reactor," M. S. Thesis, The Pennsylvania State University, 1987.
12. Kim, Sung-Tae, "The Effect of Maceral Composition and Vitrinite Reflectance on the Pyrolysis and Combustion of Pulverized Bituminous Coals," M. S. Thesis, The Pennsylvania State University, 1988.

**Table 1**  
**Analytical Data for the Coal Samples Used**

Sample No	PSOC-1501	PSOC-296	PSOC-861	PSOC-1374	PSOC-733	PSOC-736
<b>Proximate Analysis: (wt%)</b>						
% Moisture	5.80	4.18	3.66	6.76	1.75	3.23
% Ash(dry)	5.55	18.19	10.93	8.82	21.44	8.59
% Volatile Matter(daf)	43.07	44.26	38.10	36.37	34.20	28.12
% Fixed Carbon (daf)	56.93	55.74	61.90	63.63	65.80	71.88
<b>Ultimate Analysis: (wt%, daf)</b>						
% Carbon	80.49	82.09	82.65	84.77	84.81	86.70
% Hydrogen	5.27	5.70	5.42	5.55	5.36	4.88
% Nitrogen	1.55	1.82	1.18	1.58	1.44	1.40
% Total Sulfur	0.68	1.20	0.83	0.80	1.31	0.62
% Oxygen (Diff)	12.01	9.19	9.92	7.30	7.08	6.40
<b>Maceral Composition: (vol%, dmmf)</b>						
Vitrinite	92.4	41.4	60.5	93.3	48.1	24.2
Fusinite	1.9	8.3	5.4	2.2	2.6	8.2
Semifusinite	2.4	7.9	30.9	1.2	19.7	47.0
Macrinite	0.5	2.1	1.0	0.2	1.4	1.9
Micrinite	1.2	14.1	1.0	1.3	5.4	8.1
Sclerotinite	0.1	0.0	0.0	0.0	0.0	0.0
Sporinite	1.4	23.6	1.1	1.8	20.2	10.7
Resinite	0.1	2.5	0.1	0.0	2.5	0.0
Alginite	0.0	0.2	0.0	0.0	0.2	0.0
<b>H/C: (Atomic Ratio)</b>	0.7868	0.8334	0.7880	0.7863	0.7589	0.6760
<b>Mean-Max Vitrinite Reflectance (R<sub>p</sub>): (% in oil)</b>						
	0.73	0.74	0.73	0.89	0.94	0.95
<b>Description</b>	low-reflectance vitrinite-rich	low-reflectance lipinitic-rich	low-reflectance inertinite-rich	high-reflectance vitrinite-rich	high-reflectance lipinitic-rich	high-reflectance inertinite-rich

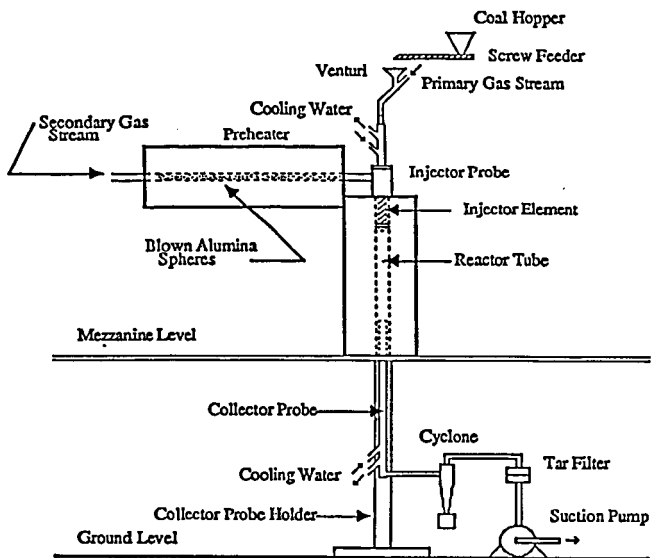


Figure 1. Configuration of Entrained-Flow Reactor and Ancillary Equipment

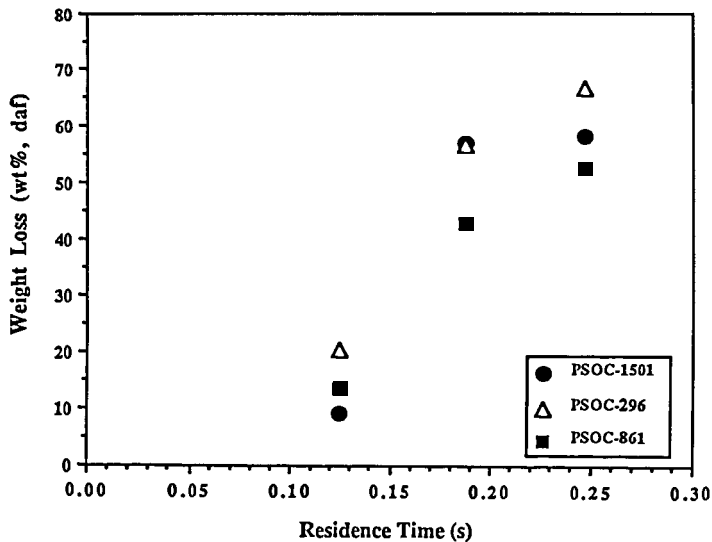
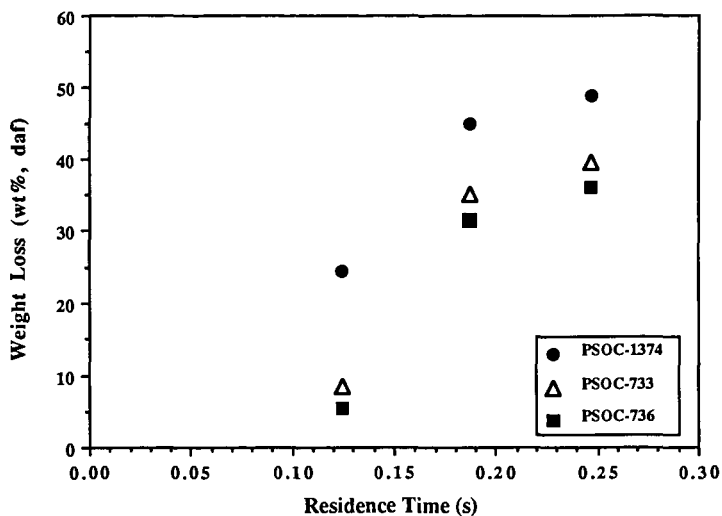
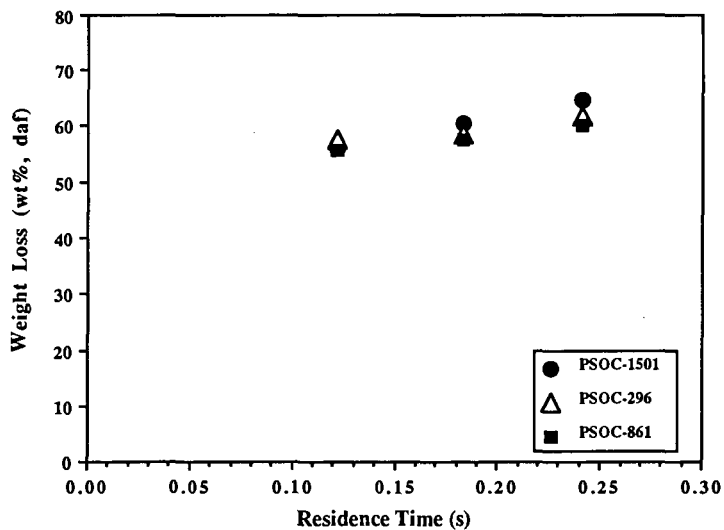


Figure 2. Effect of Maceral Composition on Weight Loss During Combustion of 100x140 Mesh Fraction of Low Vitrinite Reflectance Coals at 1073 K



**Figure 3. Effect of Maceral Composition on Weight Loss During Combustion of 100x140 Mesh Fraction of High Vitrinite Reflectance Coals at 1073 K**



**Figure 4. Effect of Maceral Composition on Weight Loss During Combustion of 100x140 Mesh Fraction of Low Vitrinite Reflectance Coals at 1273 K**

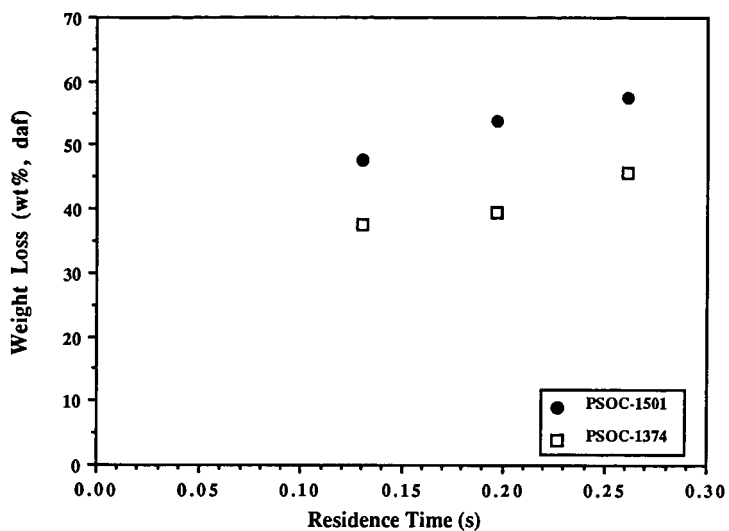


Figure 5. Effect of Vitrinite Reflectance on Weight Loss During Combustion of 140x200 Mesh Fraction of Vitrinite-Rich Coals at 1073 K

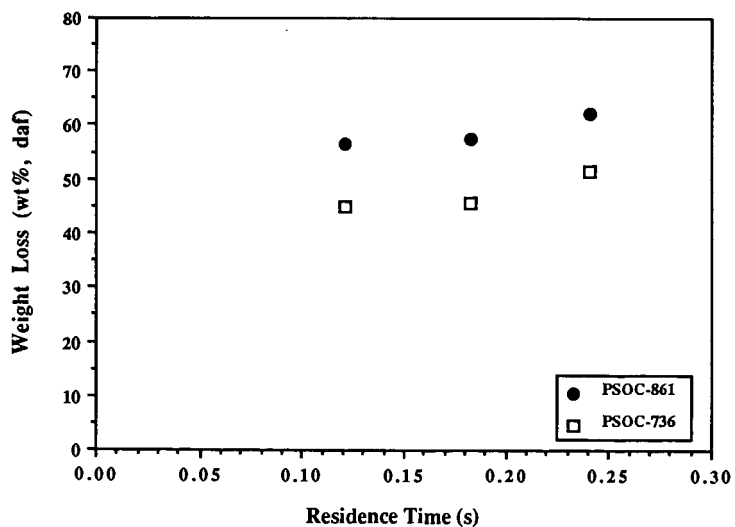


Figure 6. Effect of Vitrinite Reflectance on Weight Loss During Combustion of 100x140 Mesh Fraction of Inertinite-Rich Coals at 1273 K

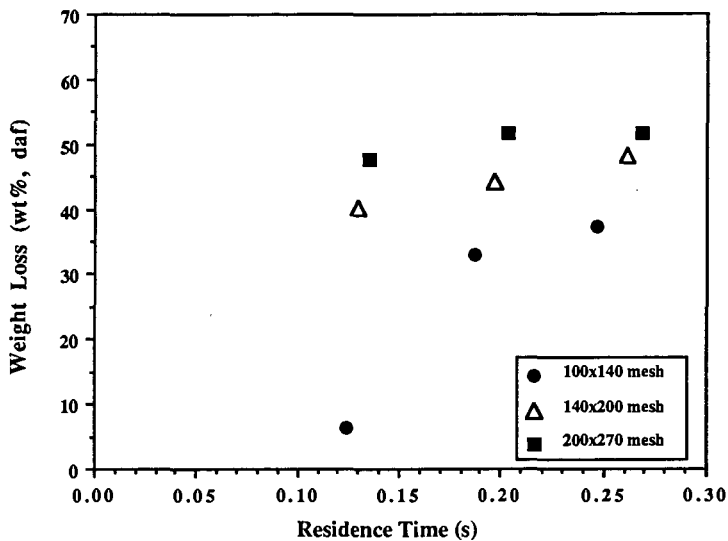


Figure 7. Effect of Particle Size on Weight Loss for Intermediate Coal (PSOC-733) During Combustion at 1073 K

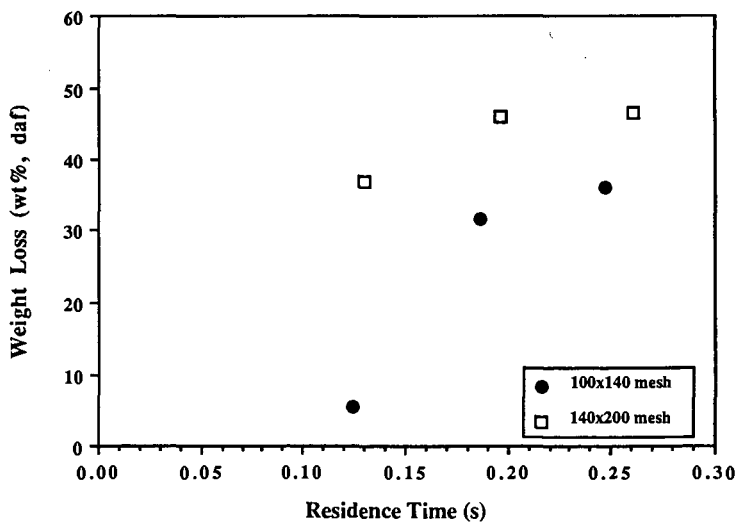


Figure 8. Effect of Particle Size on Weight Loss for Inertinite-Rich Coal (PSOC-736) During Combustion at 1073 K

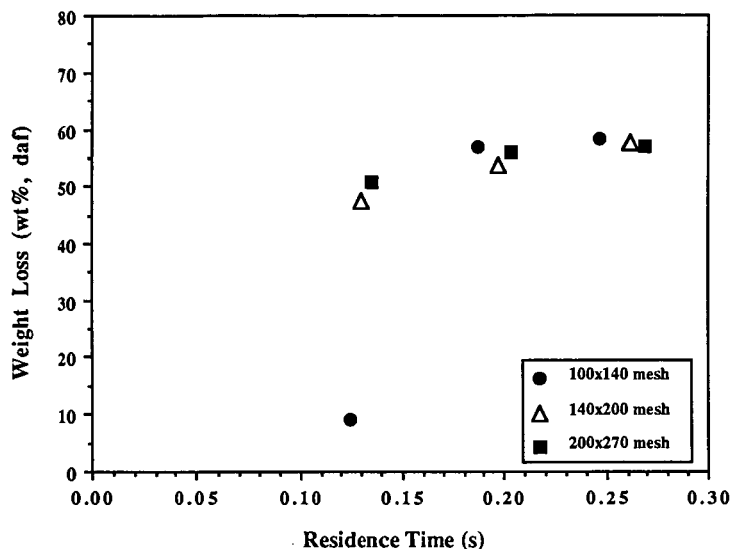


Figure 9. Effect of Particle Size on Weight Loss for Vitrinite-Rich Coal (PSOC-1501) During Combustion at 1073 K

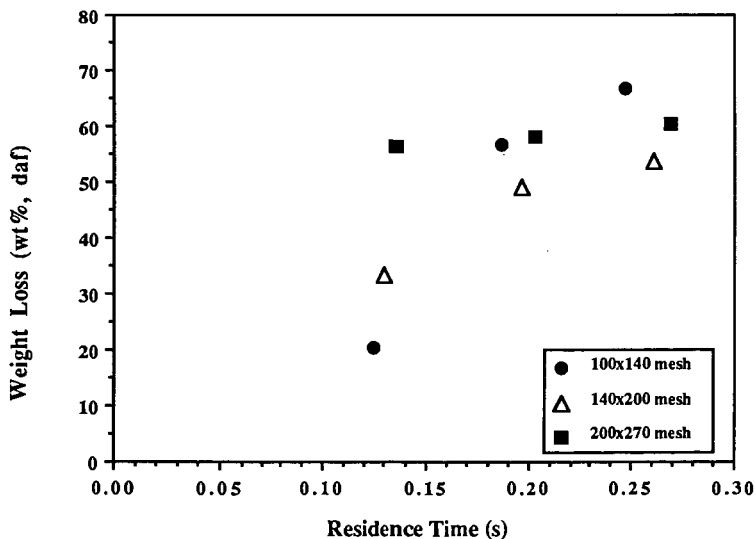


Figure 10. Effect of Particle Size on Weight Loss for Liptinite-Rich Coal (PSOC-296) During Combustion at 1073 K

## STUDIES ON IGNITION OF COAL: THE EFFECTS OF RANK, TEMPERATURE, VOLATILE CONTENT, AND LITHOTYPE

Philip G. Sweeny, Dana T. Grow\*, and Donald P. McCollor  
University of North Dakota Energy and Mineral Research Center

Box 8213, University Station, Grand Forks, North Dakota 58202

\*also Department of Chemical Engineering

### ABSTRACT

The rates of CO and CO<sub>2</sub> production from single particles of bituminous coal and lignite introduced into a hot, flowing oxidant gas stream were measured as a function of residence time. The time between injection of the particles into the combustion furnace and initial CO<sub>2</sub> production was defined as the ignition delay. These delays, as well as the maximum combustion rates and CO<sub>2</sub>:CO product ratios are reported. Two gas temperatures were employed, 923 K and 1273 K. For the bituminous coal studies, temperature was the only parameter varied. For the lignite studies, the effects of volatile content and lithotype were examined in addition to temperature. The effect of volatile matter content was ascertained by comparing a coal to its char. Ignition delays were most affected by the gas temperature, decreasing substantially with increased gas temperature. Activation energies were estimated from the ignition delays. Variations of ignition delay are discussed in terms of the ignition mechanism.

### INTRODUCTION

An important consideration in the design of coal combustion systems is ignition delay. In qualitative terms, the ignition delay can be described as the time from the combination of a fuel with an oxidant at high temperature to the beginning of the exotherm. Ignition characteristics of a given coal are important in the prevention of spontaneous ignition, in the production of stable flames, and in the establishment of optimum temperatures in fluidized bed combustion.

Several reviews of pulverized fuel combustion behavior are available (1,2,3). Parameters which affect the ignition behavior of coal and chars include rank and gas temperature. Both ignition delay and gas ignition temperature have been shown to increase with increasing coal rank (4,5). Lignite chars have been shown to be more reactive than other chars (6) and mineral matter has been found to increase the rate of combustion (7). Volatile matter has been shown to affect the mode of ignition of subbituminous and bituminous coals (8,9). Surface area has also been shown to influence ignition behavior (10). The overall objective of this study is to define the effects of moisture content, lithotype, volatile matter concentration, and mineral matter distribution on the ignition delay and combustion rate of single lignite, and subbituminous and bituminous coal particles. To date, data has been obtained from one lignite and one bituminous coal.

The most commonly monitored events used to determine ignition points are visible light production, mass loss, heat effects, and detection of products. Wall, et al. (11) have examined the correlation of light emission with combustion product formation and concluded the latter to be a better

indicator of the onset of stable combustion. Evolution of CO and CO<sub>2</sub> was chosen as the primary means of determining ignition because it is relatively unresponsive to volatile production and provides input for a mass balance.

Apparent Arrhenius activation energies and preexponential factors can be determined from gas ignition temperatures and ignition delays (4,12,13). The analysis assumes heterogeneous ignition and is accomplished through a heat balance on the particle. The unsteady-state balances have been integrated in this work to obtain Arrhenius parameters.

### UNSTEADY STATE PARTICLE TEMPERATURES

The ignition process is modeled by assuming that a spherical particle is contacted by hot gas (14,15). The particle is heated by the environment and begins to react with the oxygen present in the atmosphere. The reaction increases the particle temperature which can be substantially higher than the gas temperature. The particle temperature, as a function of time, is determined from unsteady-state energy and mass balances:

$$dm/dt = A_s \rho \quad 1)$$

$$mC_p (dT_p/dt) = A_s \rho \Delta H - hA_s (T_p - T_g) - \epsilon \sigma A_s (T_p^4 - T_w^4). \quad 2)$$

Here  $m$  is the mass of the particle, while  $A_s$  is the surface area. The energy balance equation accounts for the heating of the particle by reaction, where  $\rho$  is the overall rate of reaction and  $\Delta H$  is the enthalpy of reaction, and the loss of heat by conduction to the ambient gas and by radiation to surrounding walls. The temperatures of the particle, wall, and gas are  $T_p$ ,  $T_w$ , and  $T_g$ , respectively. The heat transfer coefficient,  $h$ , is determined from the Nusselt number,  $Nu$ , which is given by

$$Nu = hd/\lambda \quad 3)$$

The limiting value of the  $Nu$  is two and  $Nu$  depends on  $d$ , the particle diameter and  $\lambda$ , the thermal conductivity of the gas, which is a function of temperature. The emissivity,  $\epsilon$ , is taken to be unity, and  $\sigma$  is the Stefan-Boltzmann constant.

Mass and area are related to the diameter through

$$m = \pi \rho_p d^3/6 \text{ and} \quad 4)$$

$$A_s = \pi d^2 \quad 5)$$

The overall rate of combustion is determined from the rate of diffusion of oxygen to the surface,  $\rho_{diff}$ , and the rate of chemical reaction,  $\rho_{chem}$ , where these terms are given by the equations:

$$\rho_{diff} = k_{diff} (P - P_s). \quad 6)$$

where  $k_{diff}$  is given by

$$k_{diff} = 48D_o/dRT_m \quad 7)$$

and

$$\rho_{chem} = k_{chem} (P_s)^n \quad 8)$$

Here the chemical rate constant is assumed to have Arrhenius form:

$$k_{chem} = A \exp(-E/RT). \quad 9)$$

Since the surface pressure ( $P_s$ ) is unknown, an approximation employed here is to use the maximum rate of both diffusion and reaction and to calculate the overall rate from a resistances in series formula (16)

$$1/\rho = 1/\rho_{diff} + 1/\rho_{chem} \quad 10)$$

where  $n$  has been assumed to be unity. The diffusion coefficient,  $D_o$ , depends on temperature and is evaluated at the mean temperature of the particle and the gas.

The enthalpy of reaction and the heat capacity are functions of temperature and in these calculations the char particle is assumed to be composed entirely of carbon. Combustion is assumed to proceed to CO as the product, because, for short times, the temperature versus time curve is insensitive to product mix. The unsteady-state balances, Equations 1 and 2, are solved by numerical techniques to yield particle temperature versus time curves. The initial particle temperature is assumed to be 300 K. This calculation is repeated for several values of the activation energy and preexponential factor until the calculated and experimental ignition delays agree. Several temperature versus time curves are shown in Figure 1 for gas temperatures of 1273 K and 923 K.

#### EQUIPMENT AND EXPERIMENTAL PROCEDURE

The ignition apparatus was similar to that employed by Gomez and Vastola (8). A detailed side view of the ignition apparatus combustion zone is shown in Figure 2. The system includes a tube furnace with hot zone, a particle feeder, and a gas mixing system. The combustion products are measured with CO and CO<sub>2</sub> analyzers which are connected to an A/D converter and a minicomputer to collect concentration versus time data. Thermocouples monitor wall and gas temperatures. The particle feeder is a stainless steel tube and is grounded to prevent electrostatic charge accumulation. A quartz window provides optical access for the trigger system.

Coal samples were obtained from the Pennsylvania State University Sample Bank and included a Beulah lignite (PSOC-1507) and Pittsburgh #8 (PSOC-1451) bituminous coal. The lithotypes vitrain, attritus, and fusain were physically separated from the coal samples. Particles were sized under a microscope and were observed to be irregular in shape. Hence, an aspect ratio was calculated from the formula  $2a/(b+c)$ , where the axes are ordered  $a > b > c$ .

The coal or char particles are first picked up by a suction bulb and

sized under a microscope. The experiment is started by placing the particle in a syringe needle and pushing it into the drop tube with a thin wire. Data collection from the CO/CO<sub>2</sub> analyzers is started when the particle travels past the trigger. The gas flow rate through the apparatus was 200 ml/min and the gas composition was 80% N<sub>2</sub> and 20% O<sub>2</sub>. The linear velocity was 26 cm/sec.

The apparatus was calibrated using malonic acid to produce CO<sub>2</sub> at 413 K which acted as a marker to measure the time for flow between the source and the detector. Further details are available (17).

Char of the untreated lignite was produced in an air natural gas flame at approximately 3% excess oxygen. The chars were collected with a nitrogen-quenched extraction probe at 200 mm above the injection point, corresponding to a residence time of 150 ms. Gas temperature varied from approximately 1500 K at the particle injection point to 1050 K at the collection point. After collection, the chars were sieved, and size ranges were selected for combustion tests. The coals and chars were stored over concentrated H<sub>2</sub>SO<sub>4</sub> or water at 30°C for two weeks to establish relative moisture contents of 0 and 100%, respectively (18).

## RESULTS AND DISCUSSION

The CO<sub>2</sub> concentration versus time curve yields the ignition delay once the system calibration constant is known. The total carbon production is determined from the summation of the CO and CO<sub>2</sub> concentrations. The data is then differentiated to determine the gas production rate as a function of time. Examples of the rate versus time curves are given in Figures 3 and 4. The peaks in these curves give the maximum CO and CO<sub>2</sub> production rates. Arrhenius parameters were estimated by varying the E and A constants in Equation 9 to match the ignition delay time.

Water had no discernable effect on the ignition delay, combustion rate, or CO<sub>2</sub>/CO product ratio of Beulah lignite vitrain, as shown in Table 1. Lithotype had an effect on the ignition delay of Beulah lignite with fusain igniting the fastest. Karz et al. (13) have reported that fusains have shorter ignition delays than vitrains obtained from an anthracite and a bituminous coal.

The effect of volatiles on the combustion behavior of Beulah lignite can be seen by comparing the results obtained from char to those obtained from burning the parent lignite (see Table 1). The char reacted as rapidly as the most reactive lithotype and produced a similar, yet somewhat lower, maximum combustion rate. The overall CO and CO<sub>2</sub> production profiles obtained from the char did not differ significantly from those observed for the lignite shown in Figure 4. Heterogeneous ignition of the lignite is indicated since its combustion behavior is similar to that of its char, which can only ignite in a heterogeneous manner.

The effect of material rank on ignition delay and combustion rate can be seen from comparing the Beulah lignite results to those obtained from Pittsburgh #8 bituminous coal. These two materials behaved similarly at 1273 K, however, at 923 K a substantial difference was noted. At 923 K, the bituminous coal was less reactive than the lignite, exhibiting a longer ignition delay and a lower maximum combustion rate. A comparison of the

overall profiles, Figures 3 and 4, shows that the bituminous coal burns in two distinct stages as opposed to the single stage of the lignite. The two stages represent initial volatiles combustion followed by char burnout. The single stage combustion of Beulah lignite indicates that its char is highly reactive, a fact supported by the char data.

Increasing the gas temperature dramatically decreased the ignition delay time for both the Pittsburgh #8 vitrain and the Beulah vitrain. The Arrhenius activation energy is estimated to be about 20 kcal/mole for a preexponential factor of 200 g/(cm<sup>2</sup>s) when determined from the delay times. The particle temperature versus time curves for two gas temperatures calculated using Equations 1-10 are presented in Figure 1. These compare favorably with the 29.6 and 20 kcal/mole used by Bandyopadhyay and Baduri (4) for bituminous coal and lignite, respectively. In addition, Karcz et al. (13) obtained 17.6 kcal/mole from experiments on bituminous vitrain. Wall and Gururajan (12) cite a value of 17 kcal/mole for a lignite, and Patel et al. (18) used TGA to measure an activation energy of 18 kcal/mole for a char burned for 100 ms at 1030 K in a flame burner.

## CONCLUSIONS

The production of CO and CO<sub>2</sub> was measured as a function of time for several low-rank coals and chars. Detection is possible for individual particles of about 200 μm. Activation energies obtained from ignition delay times agree well with measurements from TGA experiments as well as steady-state Semenov analyses. Ignition delay depends strongly on gas temperature and, to a minor extent, on lithotype. The Beulah lignite char was demonstrated to be a highly reactive material and comparison of its ignition behavior to that of the lignite indicated that the lignite ignited heterogeneously.

## REFERENCES

1. R.H. Essenhigh in "Chemistry of Coal Utilization", M.A. Elliott, ed., John Wiley & Sons, New York, 1981, p. 1153.
2. M.F.R. Mulcahy and I.W. Smith, Rev. Pure and Appl. Chem., **19**, 81, 1969.
3. M.A. Gill, D.W. Gill, B.B. Morgan, and P.G.A. Hawksley, Combustion of Pulverised Coal, The British Coal Utilization Research Association, Leatherhead, 1967.
4. S. Bandyopadhyay and D. Bhaduri, Combustion and Flame, **18**, 411, 1972.
5. J.H. Harker and N.S. Mellor, J. Inst. Energy, **59**, 154, 1986.
6. B.C. Young and S. Niksa, Fuel, **67**, 155, 1988.
7. J.T. Ashu, N.Y. Nsakala, O.P. Majajan, and P.L. Walker, Fuel, **57**, 250, 1978.
8. C.O. Gomez and F.J. Vastola, Fuel, **64**, 558, 1985.
9. C.Y. Tsai and A.W. Scaroni, Energy and Fuels, **1**, 263.

10. J.G. Cogoli, D. Gray, and R.H. Essenhigh, Comb. Sci. Tech., 16, 165, 1977.
11. T.F. Wall, D. Phong-anat, V.S. Gurujan, L.J. Wibberley, A. Tate and J. Lucas, Combustion and Flame, 72, 111, 1988.
12. T.F. Wall and V.S. Gurujan, Comb. and Flame, 66, 151, 1986.
13. H.K. Karz, W. Kordylewski, and W. Rybak, Fuel, 59, 799, 1980.
14. M. Chen, L. Fan, and R.H. Essenhigh, Twentieth Symp. (Int.) on Combustion, The Combustion Institute, Pittsburgh, p. 237, 1984.
15. H.M. Cassel and I. Leibman, Comb. and Flame, 3, 437, 1956.
16. G.R. Thomas, A.J. Stevenson, and D.G. Evans, Comb. and Flame, 21, 133, 1968.
17. D.P. McCollor, P.G. Sweeny, and S.A. Benson "Coal/Char Reactivity Final Technical Progress Report", 1987, Cooperative Agreement #DE-FC21-86MC10637.
18. S.C. Deevi and E.M. Suuberg, Fuel, 66, 454, 1987.
19. M.M. Patel, D.T. Grow, and B.C. Young, Fuel, 67, 165, 1988.

TABLE 1  
IGNITION RESULTS FOR SEVERAL COALS AND CHARs

Material	Number of particles	I (K)	Particle Volumex, $10^{-6}$ (cm <sup>3</sup> )	Aspect Ratio	Maximum Rate $\times 10^{-6}$ (g/sec)	CO <sub>2</sub> /CO Product Ratios	Delay (ms)
Beulah Vitrain, wet	7	923	8.3 ± 1.5	1.6	3.9 ± 1.1	0.99 ± 0.21	376 ± 62
Beulah Vitrain, dry	11	923	5.4 ± 1.3	1.7	4.5 ± 1.1	0.84 ± 0.16	419 ± 51
Beulah Fusain	7	923	6.7 ± 1.9	1.8	6.3 ± 1.4	0.88 ± 0.33	302 ± 51
Beulah Attritus	9	923	9.8 ± 5.1	2.1	7.2 ± 2.7	0.78 ± 0.25	371 ± 36
Beulah Vitrain	8	1273	6.9 ± 2.0	1.7	5.3 ± 1.2	1.19 ± 0.36	137 ± 38
Pitts #8 Vitrain	7	1273	6.2 ± 1.8	1.4	4.5 ± 1.8	2.01 ± 0.53	120 ± 79
Pitts #8 Vitrain	8	923	6.5 ± 2.9	1.7	0.99 ± 0.25	--- <sup>a</sup>	480 ± 34
Beulah Char	7	923	7.4 ± 3.1	2.5	4.2 ± 2.4	1.06 ± 0.30	309 ± 63

a. Not available

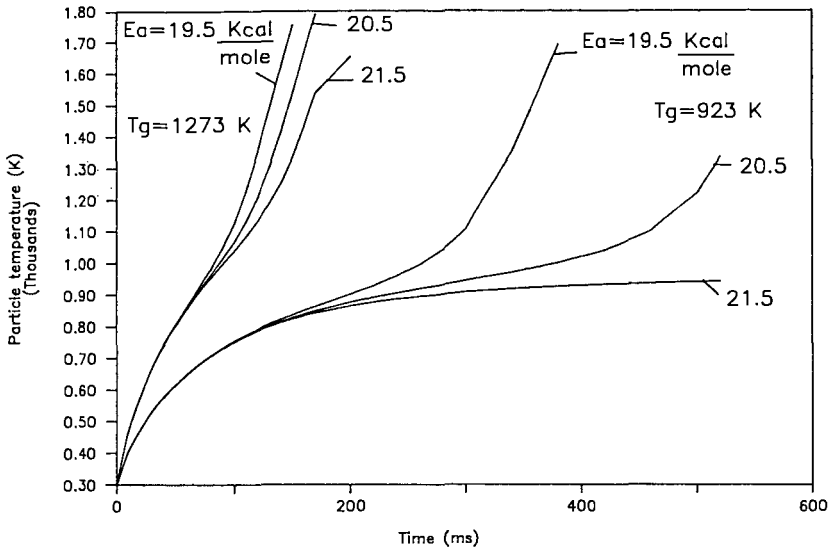


Figure 1. Calculated Temperature Profiles for 200  $\mu$ m Particles

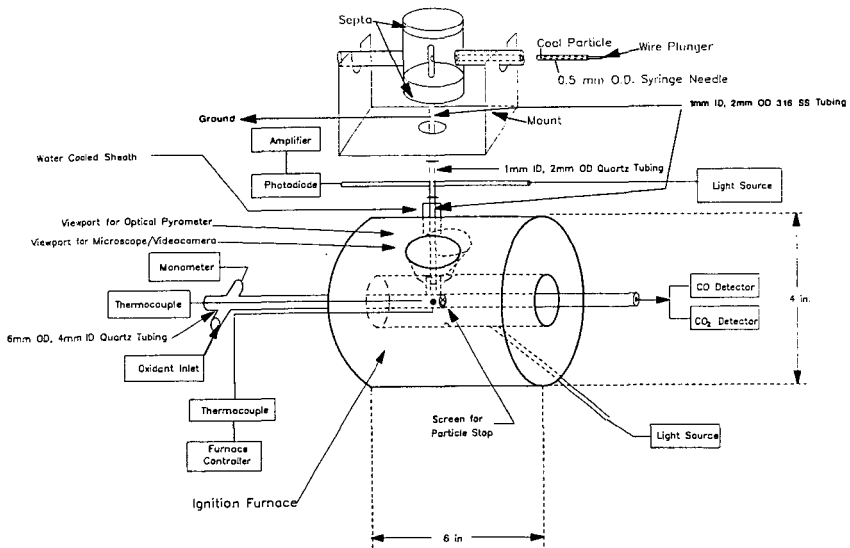


Figure 2. Detailed Side View of the Ignition Apparatus

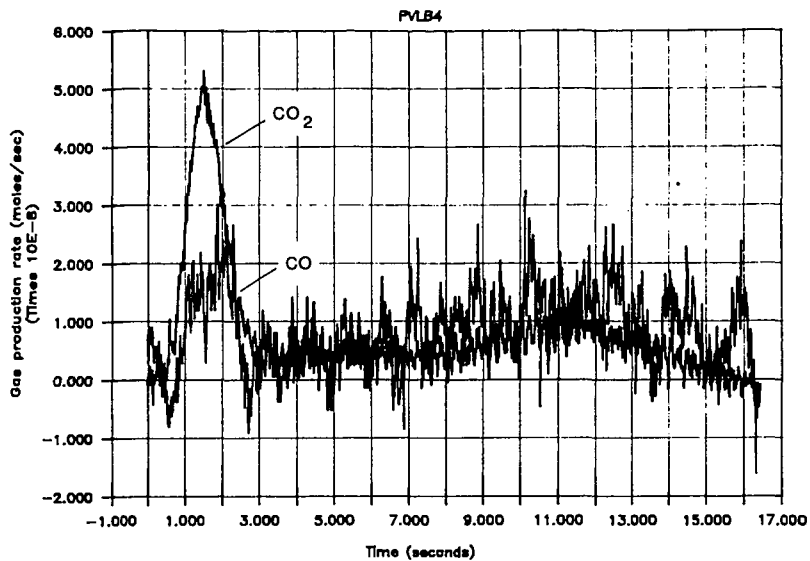


Figure 3. CO and CO<sub>2</sub> Production Rate Profiles of Pittsburgh #8 Coal at 923 K

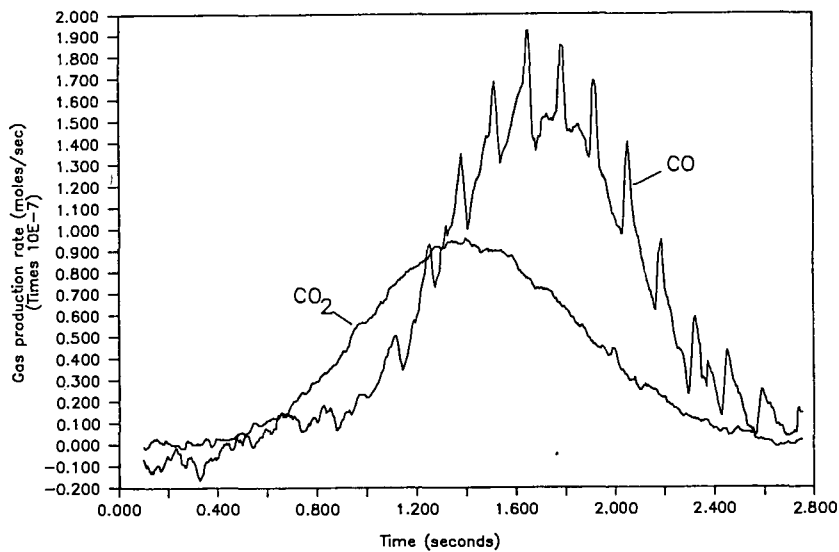


Figure 4. CO and CO<sub>2</sub> Production Rate Profiles of Beulah Lignite at 923 K

## CHANGES IN ACTIVATION ENERGY WITH LEVEL OF BURN-OFF FOR BITUMINOUS COAL CHARs

M. Rostam-Abadi, D. L. Moran, J. A. DeBarr

Illinois State Geological Survey, 615 E. Peabody Drive, Champaign, IL 61820

### INTRODUCTION

The kinetics of oxidation of coal char has been extensively studied during the last decade (1-4). A common goal of these studies has been to evaluate reactivity of char under diffusion-free conditions and to identify physico-chemical properties of a char which influence its reactivity.

Thermogravimetric analysis has been widely used to obtain rate data for the reaction char oxidation (1-7). Isothermal studies have demonstrated that the oxidation rate changes with conversion and exhibits a maximum at a specific level of burn-off. Data have been analyzed to obtain the intrinsic reactivity and activation energy for char oxidation. In most of the previous studies, however, the activation energy has been calculated at a specific conversion, usually at 50% conversion or at a level corresponding to the maximum rate. Since the value of activation energy has a pronounced effect on the intrinsic reaction rate, it seems appropriate to investigate whether activation energy changes with conversion during oxidation of coal char.

In this paper the results of a study on the oxidation of three bituminous coal chars are presented. The focus is on the variation of activation energy with level of burn-off for the three chars.

### EXPERIMENTAL

Char - Chars, also referred to as partially devolatilized (PD) coals, were made from two bituminous coal samples obtained from the Illinois Basin Coal Sample Program, samples IBCSP-3 and IBCSP-4(8). IBCSP-3 is mine-washed coal [a blend of Springfield (No. 5) and Herrin (No. 6)] and the IBCSP-4 is run-of-mine Herrin (No. 6) (see table 1 for analyses).

Two chars (char-1 and char-3) were made from two partially devolatilized (PD-1, PD-3) coals that were produced from IBCSP-3 in the United Coal Company's (UCC) Mild Gasification Pilot Unit (Bristol, Virginia). PD-1 and PD-3 had volatile matter contents of 25.6% and 13.0% (dry-ash-free basis). The details of PD coal production are given elsewhere (9). Chars were made by injecting PD coals into a 5-cm diameter batch fluidized-bed reactor which was preheated to 850°C under a purge of nitrogen. The samples were fluidized at 850°C for 5 minutes and then cooled to ambient conditions. The volatile matter content of char-1 and char-2 were 7.5% and 6.3%.

A third char, hydrodesulfurized (HDS) char, was prepared from IBCSP-4 which was first physically cleaned (14.8% ash and 6.2% S). The char was produced in the batch fluidized-bed reactor from a 74-589 micrometer-size fraction of the clean coal using the following processing steps: 1) preoxidation at 250°C in a 5% O<sub>2</sub> - 95% N<sub>2</sub> gas mixture for 30 minutes, 2) pyrolysis in nitrogen at 850°C for 15 minutes, and 3) desulfurization in hydrogen at 850°C for 90 minutes. The HDS char had 0.4% sulfur and 3% volatile matter.

Reactivity tests - The particle size of char samples was reduced to less than 90 micrometers prior to reactivity tests by crushing, and sieving and recrushing the oversize. Reactivity experiments were performed in an Omnitherm thermogravimetric analyzer (TGA) coupled to an Omnitherm QC25 programmer/controller. The TGA system was interfaced with an IBM XT computer through a Keithley DAS series 500 data acquisition system to provide automated data collection and storage.

In each experiment a sample mass of about 2 mg was placed in the TGA platinum pan and heated in nitrogen (200 cm<sup>3</sup>/min) at 50°C/min to the reaction temperature (between 425 and 575°C). The nitrogen was replaced by dry air flowing at a rate of 200 cm<sup>3</sup>/min. The percent weight of the unburned char, the rate of weight loss, and the gas temperature in the vicinity of the sample pan as a function of time were monitored by the computer. Data were collected at 5 to 40 second intervals depending on the reaction temperature.

## RESULTS AND DISCUSSION

TGA data were used to calculate the apparent reaction rates, R, where

$$R = - \frac{1}{f} \frac{df}{dt} \quad 1)$$

and

$$f = (M-M_a)/(M_o-M_a) \quad 2)$$

f = fraction combustible remaining at time t, M = mass of sample at time t, M<sub>o</sub> = initial sample mass, M<sub>a</sub> = mass of sample at complete conversion, i.e. ash. Figures 1, 2, and 3 show plots of apparent rates versus fraction conversions for the chars at the indicated temperatures. As expected, apparent rates increased with increases in reaction temperature. Also, for each char, the shape of the reactivity curve did not change with temperature. However, there are clear differences among the reactivity curves of the three chars. For char-1, apparent rate increased initially, maximized at about 30% conversion and decreased slightly as the fractional burn-off increased. For char-3, the apparent rate maximized after 5 to 15% conversion, depending on the reaction temperature, and remained relatively constant after about 30% conversion. For HDS, the apparent rates did not show a maximum and increased with conversions up to 90% conversion in the studied temperature range. These results suggest that char formation conditions influence the shape of the reactivity curve.

The differences observed in the reactivity curves could be partially due to the variations that occur in internal pore surface area during char oxidation. In order to gain information with respect to relative available pore surface area, the oxidation rate of char was expressed as:

$$- \frac{df}{dt} = SkP_{O_2}^n f \quad 3)$$

where k = reaction rate constant, g/m<sup>2</sup>.atm.min; P<sub>O<sub>2</sub></sub> = oxygen partial pressure, atm; S = available pore surface area, m<sup>2</sup>/g; n = reaction order with respect to oxygen pressure.

The initial rate of the reaction at t=0 (or f=1) is:

$$- \left( \frac{df}{dt} \right)_i = S_o k P_{O_2}^n \quad 4)$$

where S<sub>o</sub> is the initial pore surface area. Dividing equation 3) by 4) and solving for S/S<sub>o</sub> gives

$$\frac{S}{S_o} = \frac{1}{(-df/dt)_i} \frac{(-df/dt)}{f} \quad 5)$$

According to equation 5), a plot of  $(-df/dt/f)/(-df/dt)$ , versus conversion should represent changes in available surface area with conversion. Figure 4 shows how the relative available pore surface area of the samples changed with conversion. In these figures, the values of  $(df/dt/f)$  were normalized by the corresponding values at the 10% conversion because at the lower conversion levels TGA data could not be obtained accurately. For each char a single curve could adequately represent the data in the studied temperature range. A similar observation has been reported by previous investigators (1,2). This indicates that the rate data were obtained under diffusion-free conditions and surface area development was independent of reaction temperature. Each fuel demonstrates a unique pore area development. HDS which had the lowest initial internal surface area among the fuels tested (because it was subjected to most severe heat treatment condition) exhibited the largest change.

The rate data shown in figures 1, 2, and 3 were used to determine activation energies for the oxidation of the chars. The rate constant was assumed to have Arrhenius form:

$$k = k_0 e^{-E/RT} \quad 6)$$

where  $k_0$  is the pre-experimental factor and E is the activation energy (kJ/mole). Substituting equation 6) into equation 4), solving for  $(-df/dt/f)$ , and taking logarithm of both sides yields equation 7)

$$\ln(-df/dt/f) = \ln(k_0 P_{O_2}^n) + \ln S - \frac{E}{RT} \quad 7)$$

According to equation 7) a plot of  $\ln(-df/dt/f)$  versus  $1/T$  gives activation energy from the slope at a given conversion if the values of S are independent of reaction temperature.

The values of  $\ln(-df/dt/f)$  evaluated at 10%, 20%, 30%, 50%, and 70% burn-off were plotted against  $1/T$ , and are shown in figures 5, 6, and 7. The observed changes in the slopes of the plots demonstrated variations in activation energies with conversion. This is clearly seen in figure 8 where the values of activation energies are plotted against conversion. According to this figure, activation energies may increase, or may show a maximum or minimum as reaction proceeds, depending on the fuel tested. The most often reported value for the activation energy of char combustion at temperatures  $<600^\circ\text{C}$  is 130 KJ/mole (Radovic, 1983; Khan, 1987). The results obtained in this study indicate values ranging from 107 to 145 KJ/mole, depending on the fuel and the level of burn-off. Results of a recent kinetic study conducted with a sucrose char also indicated that activation energy for the oxidation of the char increased from 136 to 147 kJ/mole as conversion increased from 20 to 90% (10).

The variation in activation energy with the level of burn-off could be partly due to the presence of a distribution or type of active sites in the char with each type having its own characteristic reactivity. Past studies (11) have indicated that two types of surface oxides, stable and fleeting, are formed when oxygen chemisorbs on carbon active sites. Oxidation char is represented by several reactions including formation and desorption of surface oxides as well as direct burn-off of the carbon. These reactions may have different activation energies. Also, the contribution of each reaction to the progress of char oxidation may be significant at different levels of burn-off. This could result in variation of activation energy with conversion as observed in this study.

The results obtained in this study suggest that to more fully describe burning characteristics of a char, reactivity data should be examined at different conversions. This observation was also reported in a recent study in which an average reactivity

the whole char burn-off was used to describe char reactivity rather than one determined at a specific level of burn-off (12).

#### ACKNOWLEDGEMENTS

This work was funded in part by grants from the Illinois Coal Development Board through the Center for Research on Sulfur in Coal.

#### REFERENCES

1. Dutta, S. and C. Y. Wen, 1977, *Ind. Eng. Chem. Proc. Des. Dev.*, 16(1), 31-37.
2. Su, J. L. and D. D. Perlmutter, 1985, *AIChE J.* 31(9), 973-981.
3. Tseng, H. P. and T. F. Edgar, 1985, *Fuel*, 64(3), 373-379.
4. Sahu, R., Y. A. Levendis, R. C. Flagan and G. R. Gavalas, 1988, *Fuel*, 67(2), 275-283.
5. Radovic, L. A., and P. L. Walker, Jr., 1984, *Fuel Processing Technology*, 8, 149-154.
6. Khan, M. R., 1987, *Fuel*, 66(12), 1626-1634.
7. Solomon, P. R., M. A. Serio and S. C. Heninger, 1986, *ACD Div. Fuel Chem. preprints*, 31(3), 200-205.
8. Kruse, C. W., R. D. Harvey, and D. M. Rapp, 1987, *ACS Div. Fuel. Chem. preprints*, 32(4), 359-365.
9. Rostam-Abadi, M., 1987, *Final Technical Report to the Center for Research on Sulfur in Coal for the period September 1, 1986 - August 31, 1987*, 49 pages.
10. Floess, J. K., J. P. Longwell and A. F. Sarofim, 1988, *Energy and Fuels*, 2(1), 18-26.
11. Laine, N. R., F. J. Vastola and P. L. Walker, Jr., 1963, *J. Phys. Chem.*, 67, 2030-2037.
12. Tsai, C. Y. and A. W. Scaroni, 1987, *Fuel*, 66(10), 1400-1406.

Table 1. Chemical characterization of coal samples  
wt% (moisture-free basis)

Coals	IBCSP-3	IBCSP-4
Seam	No. 5 <sup>1</sup>	No. 6
Rank	HVBB	HVCB
Moisture	5.4	10.2
Volatile matter	39.2	30.6
Fixed carbon	52.4	31.3
Ash	8.4	38.1
Carbon	73.8	46.0
Hydrogen	4.9	3.5
Nitrogen	1.7	0.80
Oxygen	8.7	7.4
Sulfur	2.3	4.2
Chlorine	0.2	0.05
Heating value (Btu/lb)	13,437	8,492

<sup>1</sup> Predominantly Springfield (No. 5). Approximately 20% Herrin (No. 6) blended at washing plant.

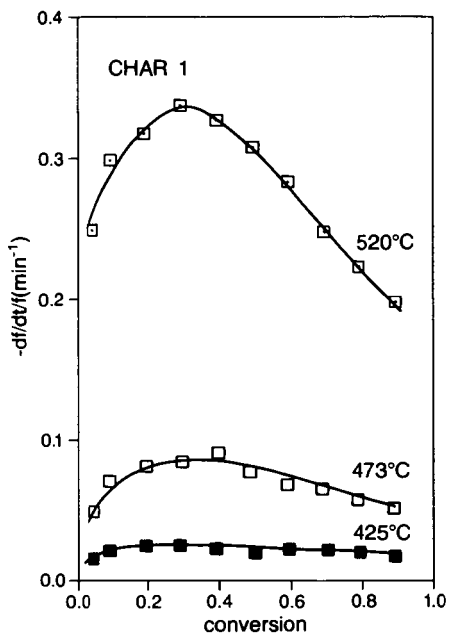


Figure 1. Apparent rate vs. conversion for oxidation of Char 1 in air.

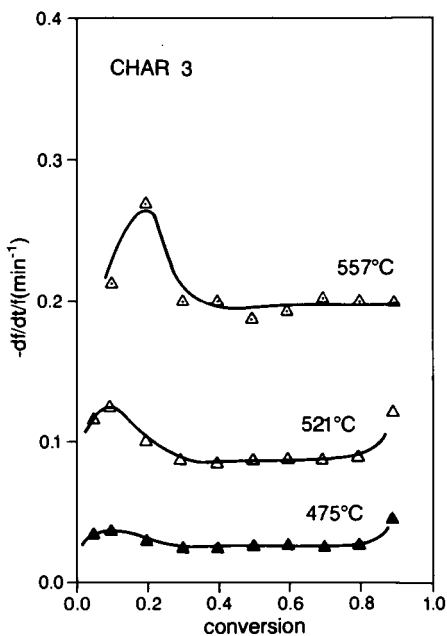


Figure 2. Apparent rate vs. conversion for oxidation of Char 3 in air.

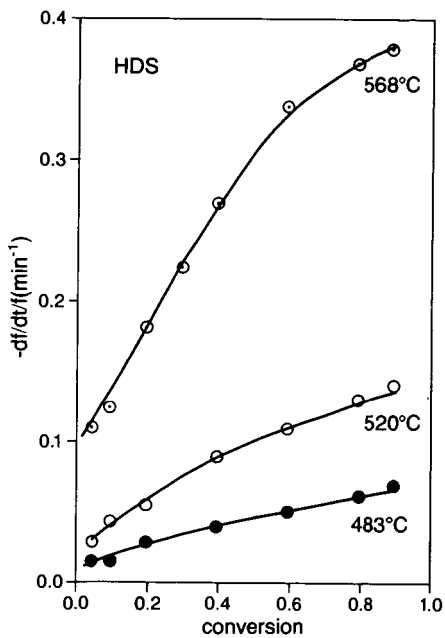


Figure 3. Apparent rate vs. conversion for oxidation of HDS char in air.

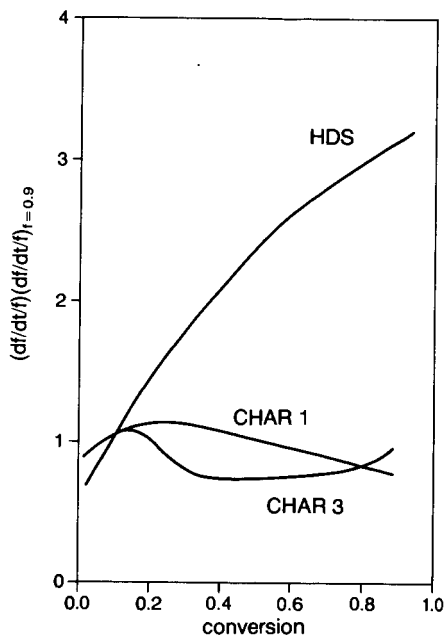


Figure 4. Surface area development vs. conversion for various chars.

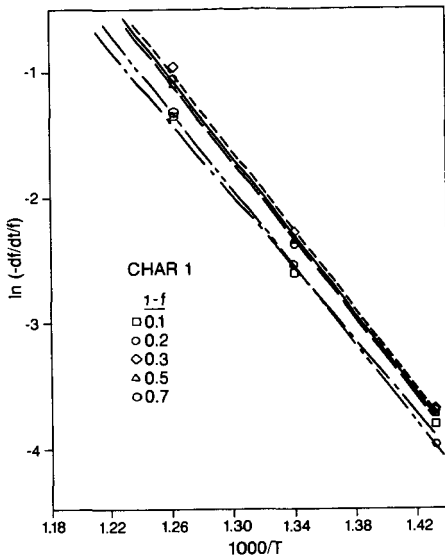


Figure 5. Arrhenius plot with rates observed at various conversions for oxidation of Char 1 in air.

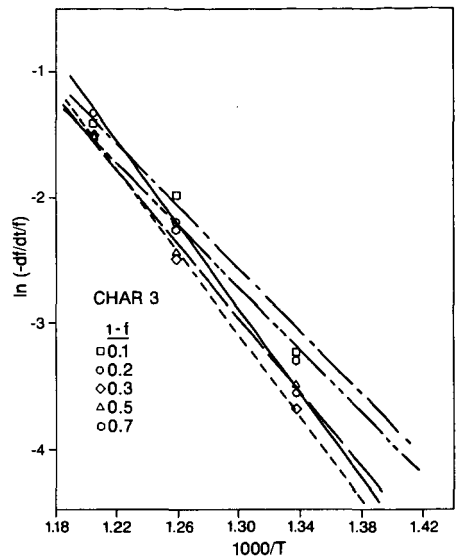


Figure 6. Arrhenius plot with rates observed at various conversions for oxidation of Char 3 in air.

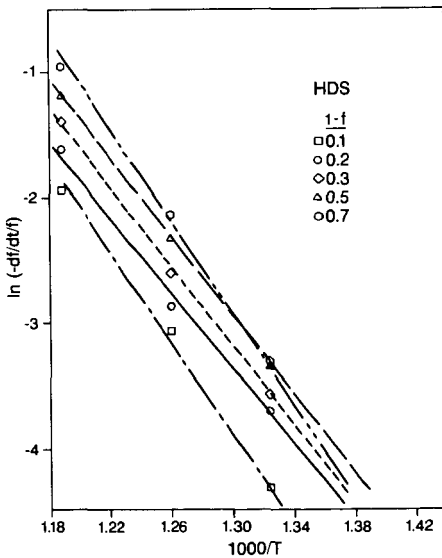


Figure 7. Arrhenius plot with rates observed at various conversions for oxidation of HDS char in air.

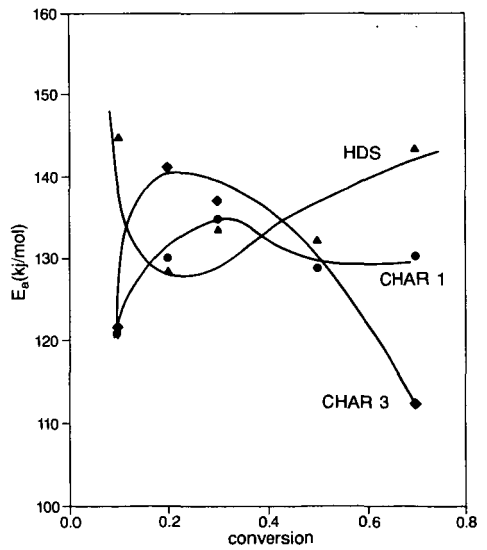


Figure 8. Variation of activation energy with conversions for oxidation of various chars.

## BURNING CHARACTERISTICS OF PARTIALLY DEVOLATILIZED COALS

M. Rostam-Abadi, J. A. DeBarr, and D. L. Moran

Illinois State Geological Survey, 615 E. Peabody Drive, Champaign, IL 61820

### INTRODUCTION

Thermal and chemical coal-desulfurization processes designed to yield refinable petroleum substitutes and solid fuels for boilers reduce the fuel's volatile matter content. This reduced volatility influences combustion characteristics such as ignition temperature, flame stability, and carbon burn-out.

A variety of studies has been conducted on the oxidation reactivity of coal char (1-5). On the basis of information available from these studies, it can be concluded that the conditions under which a char is prepared influences its reactivity. Some of the production parameters that affect the reactivity are processing gas, heating rate, maximum heat treatment temperature, soak time at peak temperature, and pressure. These factors influence the pore structure and active surface area of the char as well as the accessibility of a reactant gas to the internal surface area of the fuel during combustion or gasification. Recently it has been suggested that char formation conditions that result in a higher H/C ratio or hydrogen content favor reactivity (6-7).

The work presented in this paper is part of a larger study which was undertaken to determine combustion characteristics of partially devolatilized coals.

### EXPERIMENTAL

Char - Chars, also referred to as partially devolatilized (PD) coals, were made from a bituminous coal sample obtained from the Illinois Basin Coal Sample Program, sample IBCSP-3 (8). The analysis of the coal is given in table 1.

PD coals were made in two ways: in a pilot-scale fixed-bed reactor at the United Coal Company (UCC) located in Bristol, Virginia, and in a microbalance reactor. The UCC samples were prepared under mild gasification conditions and had volatile matter contents (dry-basis) of 23.3%, (PD-1), 15.4% (PD-2) and 11.4% (PD-3), see table 2. The details of PD production at the UCC are given elsewhere(9). The samples made in the microbalance reactor were produced under the following conditions: heating rates between 5 and 1200°C/min; heat treatment temperatures (HTT) between 400 and 900°C; soak times at maximum treatment temperatures up to 4 hours. These fuels were prepared under nitrogen purge and had volatile matter contents between 2 and 30%.

Reactivity measurement - The particle size of samples was reduced to less than 90 micrometers prior to reactivity tests. An Omnitherm Thermogravimetric Analyzer (TGA) which was interfaced with an IBM-XT computer through a Keithley DAS series 500 data acquisition system was used to obtain burning profiles of the PD coals. In each experiment, a sample mass of about 2 mg was loaded in the TGA platinum pan and was heated at a constant heating rate of 20°C/min in air from ambient to temperatures up to 800°C. The flow rate of air was 200 cc/min (STP).

### RESULTS AND DISCUSSION

Burning profile - The term burning profile was first used twenty years ago to refer to a plot of the rate of weight loss versus temperature when a small amount of coal-derived fuel is heated (usually 15-20°C/min) in air(10). Characteristic temperatures from the burning profile corresponding to the onset of burning, peak burning rate and complete burn-out were taken as a measure of a fuel's reactivity, with lower characteristic temperatures indicating more easily burned fuels. The test was used

with past experience and standard reference profiles to predict conditions, such as residence time or excess air, necessary for complete combustion of fuels in large furnaces. The burning profiles were found especially useful for evaluating combustion characteristics of unknown fuels when only small quantities of fuel were available.

In recent years, the concept of burning profiles has been used in coal combustion studies to show the effect of variations in coal rank on reactivity (11), to show the influence of maceral composition on combustion of pulverized coal (11, 12) and to determine the activation energy for oxidation of char (6, 7, 13).

Figure 1 shows typical weight loss and rate of weight loss data obtained in air for coal. The gain in sample weight between 200 and 300°C is due to oxygen chemisorption, i.e., preignition oxidation. A major weight loss began at 375°C ( $T_I$ ). This temperature was taken at the point where the rate of weight loss was 1%/min. The rate of burning peaked at 490°C ( $T_P$ ) and the coal was completely burned at 630°C ( $T_B$ ). The burn-out temperature was taken at the point where the rate of weight loss was 1%/min. The weight remaining at 650°C was the ash content of the sample which was approximately 12%.

Combustibility of coal and PD coals - The burning profiles obtained for the coal, PD-1, PD-2, and PD-3 coals are shown in figure 2. The profiles are offset to avoid overlap. The onset of burning was about 375°C for all the samples. However, there are clear differences among the burning profiles. Raw coal exhibited a single-burn profile, while double-burn profiles were observed for PD-1, PD-2 and PD-3. The second burn appeared as a shoulder peak for PD-1 and became more pronounced for PD-2 and PD-3. The double-burn behavior observed for the PD coals suggested the presence of at least two types of combustibles in the fuels. The two portions of combustibles burned in two distinct stages with peak burn rates at approximately 500°C and 550°C. The higher reactivity constituent (low temperature burn) was a coal-like material and was present in larger concentration in PD-1 followed by PD-2 and PD-3 (9). It had burning properties similar to that of the coal. Fuels with higher volatile matter content burned more rapidly. For example at 500°C, the amount of combustible materials burned (not shown) was 70% for the raw coal, 55% for PD-1, 40% for PD-2, and 20% for PD-3. The most pronounced impact of the volatile matter was on burn-out temperatures which were 580, 630, 660 and 690°C for the coal, PD-1, PD-2 and PD-3, respectively. The results indicate that under the conditions used, raw coal was the most readily combusted fuel, followed by PD-1, PD-2 and finally PD-3.

Burning profiles of PD-2 and two 15% volatile PD coals are shown in figure 3. LTC was produced in the microbalance reactor by heating the coal at 5°C/min to 525°C. Coal+HTC was a mixture of coal and a high temperature char (HTC, 3% volatile matter) which was prepared by heating the coal at 5°C/min to 850°C, see table 2. The profiles for the coal and the HTC are also shown in figure 4. LTC exhibited a single burn behavior during burning in contrast with PD-2 and Coal+HTC which exhibited double-burn behavior. The peak burn rate for the HTC occurred at 575°C which was 25°C higher than the temperature of the second burn observed for PD-2. This was because the HTC was subjected to higher processing temperature than PD-2. The burning profile for the Coal+HTC reveals that the two fraction of this fuel, i.e. coal and the HTC, burned in two stages with peak burn temperatures corresponding to those of the coal and the HTC. LTC was more reactive than PD-2 and the Coal-HTC fuel because it had a lower burn-out temperature. These results indicate that a fuel with inherent volatile matter is more reactive than a fuel with comparable volatile matter prepared by blending raw coal and low volatile char. This suggests that volatile matter alone cannot be used as an index of reactivity.

The influence of volatile matter on characteristic temperatures of PD coals which were made in the microbalance reactor are shown in figure 4. These fuels exhibited a single burn profile during combustion. The results show that there were only slight differences in characteristic temperatures for fuels with volatile matter contents above 10%. However, with further decreases in volatile matter, burn-out temperatures

increased markedly. The burn-out temperatures were particularly sensitive to preparation conditions of a sample. Fuels prepared at the fastest heating rate, i.e. 1200°C/min, and shorter soak times were more reactive and had lower burn-out temperatures than those made at slower heating rates and longer soak times. These observations are in agreement with results reported in a previous study on the reactivity of PD coals derived from an Illinois hvB coal (1). The values of  $T_B$  for PD coals prepared at UCC are also shown in figure 4. It is clearly seen that these samples had higher burn-out temperatures than those prepared in the microbalance reactor under controlled pyrolysis conditions. The UCC samples were produced in a pilot-scale reactor and were subjected to different processing conditions than the PD coals made in the microbalance reactor.

## CONCLUSIONS

Results obtained in this study suggest that PD coals with comparable volatile matter content produced from the same coal but under different processing conditions had different burning characteristics. Lower preparation temperatures, higher heating rates and shorter soak times at final pyrolysis temperatures favored reactivity. PD coals with inherent volatile matter were more reactive than fuels with comparable volatile matter prepared by blending low volatile char and the coal. It was also concluded that volatile matter alone may not be a valid index of reactivity.

## ACKNOWLEDGEMENTS

We gratefully acknowledge the Illinois Coal Development Board and the Center for Research on Sulfur in Coal for their financial support of this project.

## REFERENCES

1. Jenkins, R. G., S. P. Nandi, P. L. Walker, 1973, *Fuel*, 52(10), p. 288-293.
2. Dutta, S., C. Y. Wen, 1977, *Ind. Eng. Chem. Process Des. Dev.*, 16(1), 31-37.
3. Radovic, L. R., P. L. Walker, Jr., 1984, *Fuel Processing Technology*, 8, 149-154.
4. Wells, W. F., S. K. Kramer, L. D. Smoot, A. U. Blackham, 1984, a paper presented at the 20th International Symposium on Combustion, Ann Arbor, MI, August 12-17.
5. Katta, S., D. L. Keairns, 1984, a paper presented at AIChE meeting, Anaheim, CA, May 20-24.
6. Solomon, P. E., M. A. Serio and S. G. Heninger, 1986, *ACS Div Fuel Chem.*, 32(3), 200-205.
7. Khan, M. R., 1987, *ACS Div Fuel Chem. preprints*, 32(1), 298-309.
8. Kruse, C. W., R. D. Harvey, and D. M. Rapp, 1987, *ACS Div. Fuel. Chem. preprints*, 32(4), 359-365.
9. Rostam-Abadi, M., J. A. DeBarr, D. L. Moran and C. W. Kruse, 1987, Final Technical Report to the Center for Research on Sulfur in Coal for the period September 1, 1986 - August 31, 1987, 49 pages.
10. Wagoner, C.L. and A. F. Duzy, 1967, Paper presented at Winter Annual Meeting, ASME, Pittsburgh, PA, Nov. 12-16.
11. Morgan, P. A., S. D. Robertson and J. F. Unsworth, 1986, *Fuel*, 65(11), 1546-1551.
12. Morgan, P. A., S. D. Robertson and J. F. Unsworth, 1987, *Fuel* 66(2) 210-215.
13. Cumming, J. W., 1984, *Fuel*, 63(1), 1436-42.

Table 1. Analysis of coal, wt% (moisture-free basis)

Coals	IBCSP-3
Seam	No. 5 <sup>1</sup>
Rank	HVBB
Moisture	5.4
Volatile matter	39.2
Fixed carbon	52.4
Ash	8.4
Carbon	73.8
Hydrogen	4.9
Nitrogen	1.7
Oxygen	8.7
Sulfur	2.3
Chlorine	0.2
Heating value (Btu/lb)	13,437

<sup>1</sup> Predominantly Springfield (No. 5). Approximately 20% Herrin (No. 6) blended at washing plant.

Table 2. Volatile Matter Content of PD Coals and Their Preparation Conditions

Sample	Reactor Type	Temperature (°C)	Residence Time (hr)	Volatile Matter (%)
PD-1	Fixed Bed	760*	1.7	23.3
PD-2	Fixed Bed	760*	2.5	15.4
PD-3	Fixed Bed	760*	3.2	11.4
LTC	Microbalance	525	---	15.0
HTC	Microbalance	850	0.5	3.0
Coal+HTC				17.0

\* Reactor tube (8-inch in diameter) was located in a natural gas fired furnace kept at 760°C.

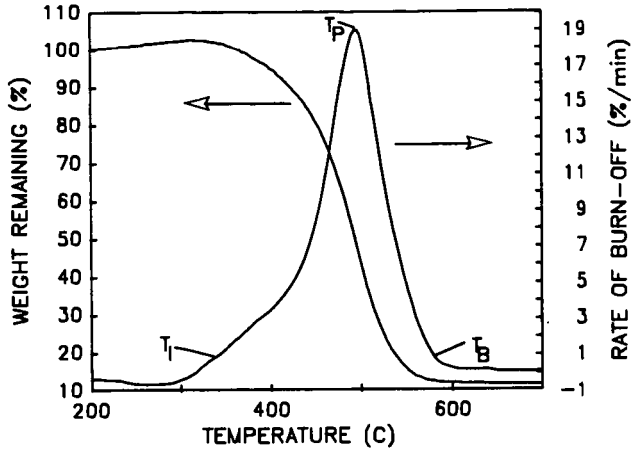


Figure 1. Burning characteristic of coal.

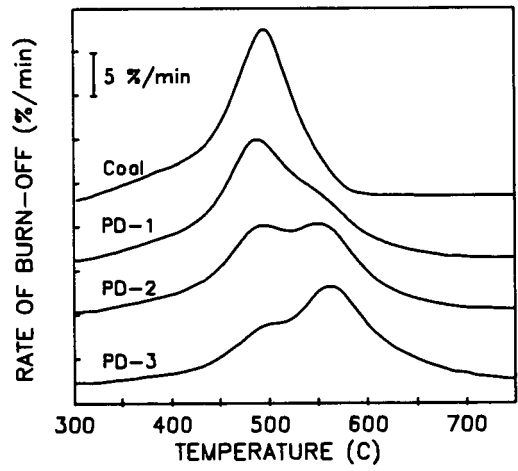


Figure 2. Burning profiles for coal and UCC PD coals

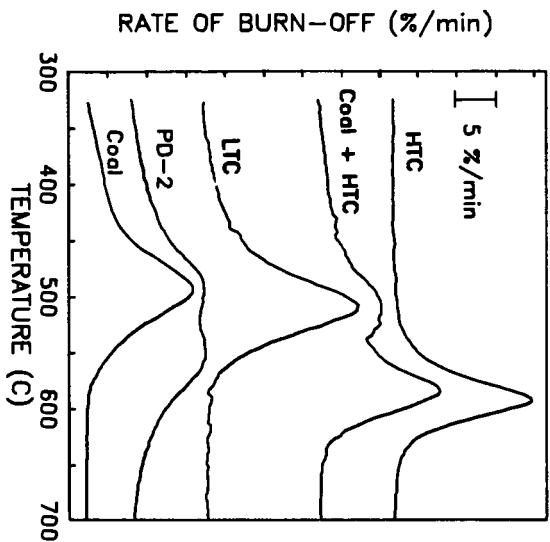


Figure 3. Burning profiles for coal, high and low temperature chars, and a mixture.

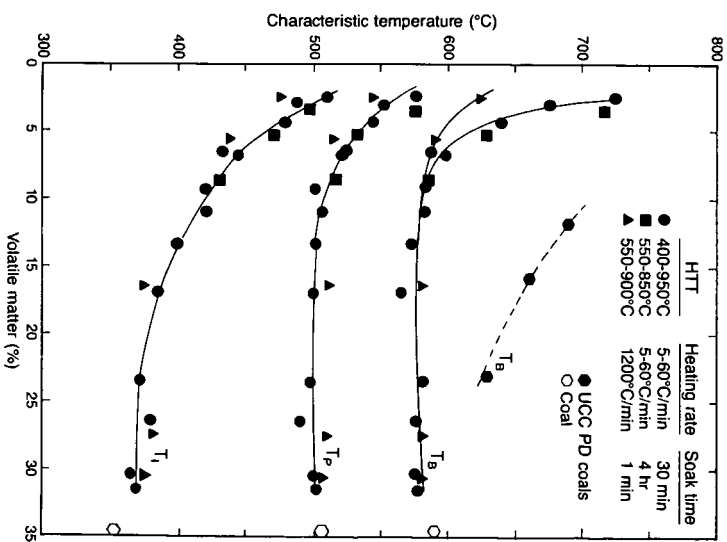


Figure 4. Effect of volatile matter on characteristic burning temperatures of chars produced under varying conditions.

## EXPERIMENTAL VERIFICATION OF THE THERMODYNAMIC PROPERTIES OF A JET-A FUEL

Carmen M. Gracia-Salcedo, Bonnie J. McBride, Theodore A. Brabbs

NASA Lewis Research Center, Cleveland, Ohio 44135

### INTRODUCTION

Thermodynamic properties for Jet-A fuel are needed for many calculations, including chemical equilibrium calculations. To fulfill this need, various correlations for the estimation of these properties have been published (1,2,3). However, these are difficult to use and may not be practical for all applications. In 1970, Shell Development Company, under a contract for NASA Lewis Research Center, determined the thermodynamic properties for a Jet-A fuel (4). In the present report, we used these thermodynamic data to derive the coefficients necessary to include Jet-A (gaseous and liquid phases) in the thermodynamic data library of the NASA Lewis Chemical Equilibrium Program (5). To verify the thermodynamic data and the polynomial fit, the temperatures of very rich mixtures of Jet-A and nitrogen were measured and compared to those calculated by the chemical equilibrium program.

### THERMODYNAMIC DATA AND LEAST SQUARES FIT

To include Jet-A in the thermodynamic data library of the NASA Lewis Chemical Equilibrium Program (5), the thermodynamic functions specific heat  $C_p^\circ$ , enthalpy  $H_T^\circ$ , and entropy  $S_T^\circ$ , need to be expressed as functions of temperature in the form of a fourth order polynomial for  $C_p^\circ$ , with integration constants for  $H_T^\circ$  and  $S_T^\circ$ .

$$\frac{C_p^\circ}{R} = a_1 + a_2 T + a_3 T^2 + a_4 T^3 + a_5 T^4 \quad 1)$$

$$\frac{H_T^\circ}{RT} = a_1 + \frac{a_2 T}{2} + \frac{a_3 T^2}{3} + \frac{a_4 T^3}{4} + \frac{a_5 T^4}{5} + \frac{a_6}{T} \quad 2)$$

$$\frac{S_T^\circ}{R} = a_1 \ln T + a_2 T + \frac{a_3 T^2}{2} + \frac{a_4 T^3}{3} + \frac{a_5 T^4}{4} + a_7 \quad 3)$$

The thermodynamic data for a Jet-A fuel used for this report were measured or calculated by Shell Development Company in 1970. Most of these data were in an extensive unpublished table provided to NASA Lewis Research Center by Shell. Part of the data contained in this table and additional fuel information used for this report were published in reference 4. The data used from reference 4 include: heat of combustion value used to calculate the heat of formation of the liquid, and a fuel analysis by hydrocarbon type and carbon number used to estimate the entropy of the gaseous fuel mixture at 298K. The data used

from the unpublished table include: heat capacity and enthalpy values for gaseous Jet-A for temperatures from 273K to 1273K, the entropy and enthalpy of vaporization at 298K, and enthalpies for liquid Jet-A for temperatures from 298K to 650K. The values for enthalpy given in this table were referenced to liquid Jet-A at 273K. The chemical equilibrium program requires an assigned enthalpy value at 298K equal to the heat of formation. For this reason, the enthalpy values from the unpublished table were adjusted to be relative to the enthalpy at 298K.

The entropy values given in Shell's unpublished table were referenced to liquid Jet-A at 273K. The chemical equilibrium program requires the entropy to be zero at 0 K. To estimate the entropy for the gaseous Jet-A, the fuel analysis given in Table XVI of reference 4 was used along with the entropy values of the individual components from reference 6. The entropy of vaporization at 298K was obtained from Shell's unpublished table and subtracted from the gas phase entropy to obtain the entropy at 298K for the liquid phase.

An updated version of the PAC4 computer code (7), namely PAC87 was used to extrapolate the thermodynamic functions for the gas to 6000K (8) and fit  $C_p$  and  $H_T$  simultaneously using a least squares method. The data were fitted in two temperature intervals, 298K to 1000K and 1000K to 5000K.

For the liquid Jet-A, the heat capacity values in the unpublished table did not match the enthalpies for temperatures above 600K. Since the enthalpy was the property measured by Shell Development Company (4), it was used in the PAC87 computer code to obtain heat capacity and entropy values for the temperature range 298K to 650K.

The chemical formula  $C_{12}H_{23}$  was used to represent Jet-A in the computer program. This results in a molecular weight of 167.3. A value of 166 was reported in reference 4.

The coefficients obtained for the liquid and gaseous phases are the following:

LIQUID: 298K≤T≤650K	GAS: 298K≤T≤1000K	GAS: 1000K≤T≤5000K
a <sub>1</sub> = 0.13993639E 04	a <sub>1</sub> = 0.19935137E 01	a <sub>1</sub> = 0.24875975E 02
a <sub>2</sub> = -0.13440366E 02	a <sub>2</sub> = 0.13383918E 00	a <sub>2</sub> = 0.78259103E-01
a <sub>3</sub> = 0.48492245E-01	a <sub>3</sub> = -0.82891249E-04	a <sub>3</sub> = -0.31556353E-04
a <sub>4</sub> = -0.75524882E-04	a <sub>4</sub> = 0.31180914E-07	a <sub>4</sub> = 0.57891394E-08
a <sub>5</sub> = 0.43166687E-07	a <sub>5</sub> = -0.71528712E-11	a <sub>5</sub> = -0.39838032E-12
a <sub>6</sub> = -0.15588486E 06	a <sub>6</sub> = -0.35903496E 05	a <sub>6</sub> = -0.43110507E 05
a <sub>7</sub> = -0.54852414E 04	a <sub>7</sub> = 0.27744570E 02	a <sub>7</sub> = -0.93633944E 02

## VERIFICATION

### Experimental Apparatus

Experiments were conducted in the vaporization section of a catalytic flow-tube reactor described in reference 9. Open-end

J-type thermocouples were used to monitor the gas mixture temperature. They were located at 46, 53, 61 and 68 cm from the point of fuel injection.

Two fuel injector designs were used in this work (see Figure 1). Both consisted of seven 10-cm long conical nozzles arranged with six in a circle and one in the center. Fuel was delivered to each cone through tubes of equal length and of 0.04 cm ID. These tubes were located to spray the fuel in the direction of the gas flow. The fuel distribution through the fuel injectors was examined and was found to be uniform within 7% for fuel injector A and 4% for fuel injector B. A nitrogen purge in the fuel line was required to remove any residual fuel in the fuel tubes before shut-down. This eliminated clogging of these small tubes.

#### **Operating Procedure**

Nitrogen is heated to about 800K with an electric heater. The standard operating procedure was to warm-up the reactor for about two hours with hot nitrogen to attain a steady state temperature. Then, liquid fuel is added and the mixture temperature 68 cm downstream of the point of fuel injection was monitored. No data was recorded until the temperature was steady for about 5 minutes. This took about 30 minutes for the first point. Then the fuel flow was increased or decreased, and data were taken in the same manner. For the second point on, data could be taken every 10 minutes.

#### **Experimental Approach**

The objective of this study is to verify the thermodynamic properties of a Jet-A fuel by measuring the temperatures of very rich vaporized fuel/nitrogen mixtures. In a prior study (9) it was observed that the addition of large quantities of liquid fuel to a high temperature gas stream caused a large reduction in the stream temperature (200 to 300K). This mixture temperature can be calculated using the chemical equilibrium program and the thermodynamic properties of the fuel (liquid and gas) and nitrogen. We found that in such a system, the temperature was very dependent upon the thermodynamic properties of the fuel. For example, a  $\pm 5\%$  change in the gas phase heat capacity of the fuel caused a  $\mp 7\text{K}$  change in the calculated mixture temperature.

First, the feasibility of the experimental technique will be demonstrated by studying iso-octane, a fuel for which the thermodynamic properties are well known. Second, the data for iso-octane will be used as a standard for determining any non-adiabatic behavior of the apparatus. Finally, Jet-A will be studied under identical conditions.

#### **Results and Discussion**

The initial data were taken with iso-octane and fuel injector A. Temperatures of fuel/nitrogen mixtures were measured for different amounts of fuel injected into the hot nitrogen stream. These measurements were compared to the temperatures

calculated by the chemical equilibrium program for 298K liquid fuel and 800K nitrogen. Since the experimental fuel and nitrogen temperatures could not be maintained at exactly these conditions, small corrections were required to reduce these to the same starting conditions. The data for iso-octane are shown in Figure 2. It was observed that for low fuel mole fractions the experimental temperatures were below the calculated ones. This behavior is expected when the experimental apparatus is not adiabatic. However, at higher fuel mole fractions, the measured temperatures were much higher than the calculated ones and tended to level off. This suggests that complete vaporization had not been obtained at the monitoring station 68 cm downstream of the point of fuel injection. In discussions with Ingebo (10), it was suggested that vaporization could be improved by increasing the gas velocity and providing a constant area section to account for the stream break-up distance (about 2.5 cm). Injector A was modified by attaching a 3.0 cm addition at the inlet of each nozzle, as shown in Figure 1b. The calculated drop size obtained with the modified fuel injector is about 22  $\mu\text{m}$ . With the previous design, calculated fuel drops were about 44  $\mu\text{m}$  at the throat of the nozzles, but droplets 2.5 times larger were calculated at a distance 2.5 cm downstream of the throat. These modifications should significantly improve vaporization.

Fuel injector B proved to be very successful, as shown by the iso-octane data in Figure 3. All the experimentally measured temperatures were below the calculated curve and the data showed a similar shape. This suggests that vaporization was complete. The temperature difference can be attributed to apparatus heat losses. These heat losses increase as the mixture temperature increases, which is the behavior expected for a non-adiabatic system. A curve fit to the experimental data indicated a heat loss varying from 7 degrees at 460K to 23 degrees at 580K. The system was calibrated by plotting the difference between this curve and the calculation as a function of temperature.

The measured temperatures for Jet-A/nitrogen mixtures are shown in Figure 4a. The behavior is exactly that observed for the iso-octane data. Correcting the experimental data points for the heat losses from the calibration curve produced the results shown in Figure 4b. These data are in excellent agreement with the temperatures calculated using the coefficients derived from the thermodynamic data for Jet-A.

The extent of vaporization of a fuel with an end boiling point of 532K (4) was checked by using the Clapeyron equation which relates the boiling temperature (T) of a liquid with its vapor pressure (P),

$$\ln P = A + B/T \quad 4)$$

Data of vapor pressure reported in reference 4 were used to determine the constants A and B. The line obtained from the equation is shown in Figure 5. The region under the line (region

I) corresponds to only vapor present, and the region above the line (region II) corresponds to liquid and vapor. Data points for the experimentally measured temperatures and partial pressures fall in region I, indicating complete vaporization of the fuel.

#### CONCLUSIONS

An experimental technique has been described in which the temperatures of very rich fuel/nitrogen mixtures were measured. These temperatures were shown to be dependent on the thermodynamic properties of the fuel. Iso-octane was used to test the feasibility of the technique and to calibrate the apparatus for heat losses. Coefficients were derived from thermodynamic data so that a Jet-A fuel could be included in the NASA Lewis chemical equilibrium program. The experimental data obtained for Jet-A in our calibrated apparatus were in excellent agreement with the calculated temperatures, confirming the correctness of the coefficients for the polynomials used in the program. This experimental technique is an excellent tool for verifying the thermodynamic properties of any multi-component fuel.

#### REFERENCES

1. "Technical Data Book - Petroleum Refining", Fourth Edition, American Petroleum Institute.
2. Maxwell, J. B.: "Data Book on Hydrocarbons", 1957.
3. "Handbook of Aviation Fuel Properties", CRC Report No. 530, Coordinating Research Council, Inc., 1983.
4. Faith, L. E., Ackerman, G. H. and Henderson, H. T.: "Heat Sink Capability of Jet-A Fuel: Heat Transfer and Coking Studies." NASA CR-72951, July 1971.
5. Gordon, S., and McBride, B. J.: "Computer Program for Calculation of Complex Chemical Equilibrium Compositions, Rocket Performance, Incident and Reflected Shocks, and Chapman-Juguet Detonations." NASA SP-273, 1976.
6. "Selected Values of Properties of Hydrocarbons and Related Compounds", Thermodynamic Research Center, Texas A & M.
7. McBride, B. J., and Gordon, S.: "Fortran IV Program for Calculation of Thermodynamic Data." NASA TN D-4097, 1967.
8. Wilhoit, R. C.: Thermodynamics Research Center Current Data News, Vol. 3, No. 2, 1975.
9. Brabbs, T. A.: "Fuel-Rich Catalytic Preburner for Volume Limited Hydrocarbon Scramjet." NASA TM-87111, 1985.
10. Private communication with Robert Ingebo, NASA Lewis Research Center, Cleveland, Ohio.

Figure 1 - Fuel Injectors

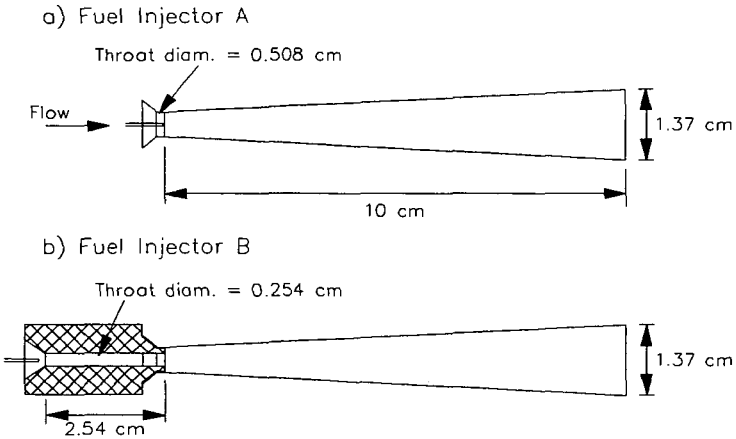


Figure 2 - Experimental Data for Iso-Octane (Fuel Injector A)

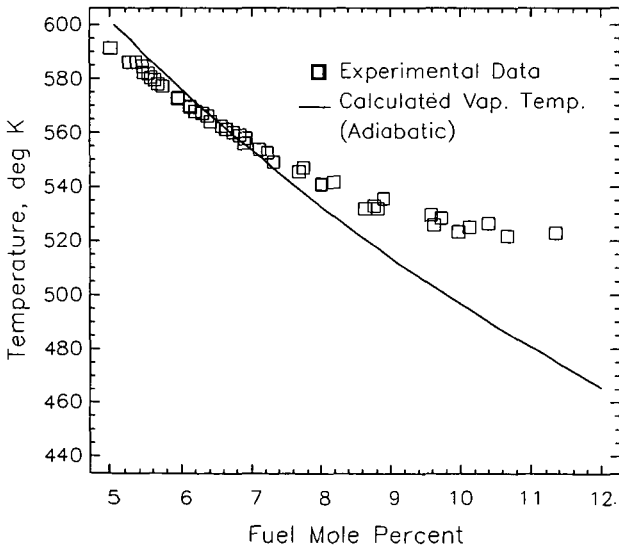


Figure 3 – Experimental Data for Iso-Octane (Fuel Injector B)

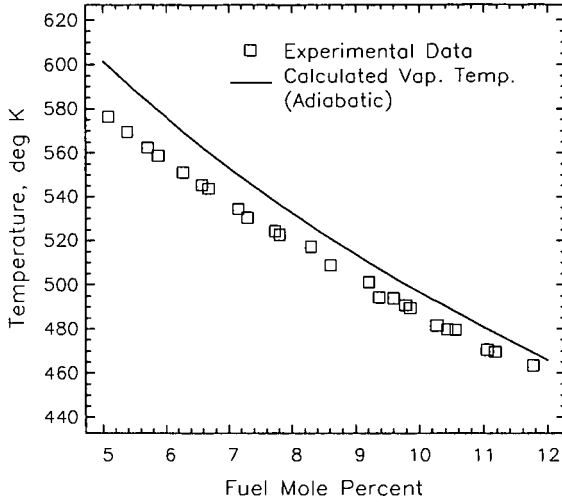
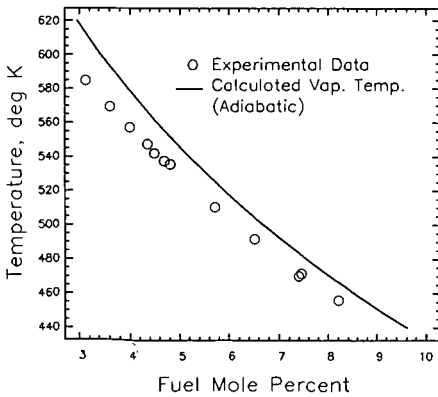


Figure 4 – Experimental Data for Jet-A (Fuel Injector B)

a) Raw Data



b) Data Corrected for non-adiabatic conditions

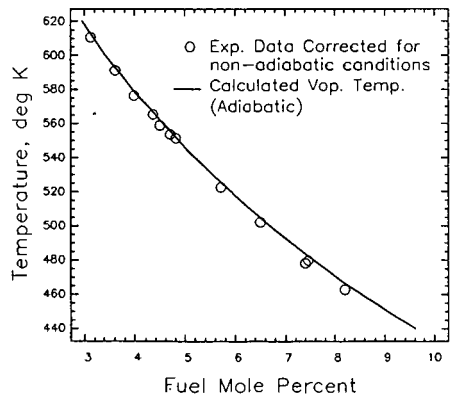
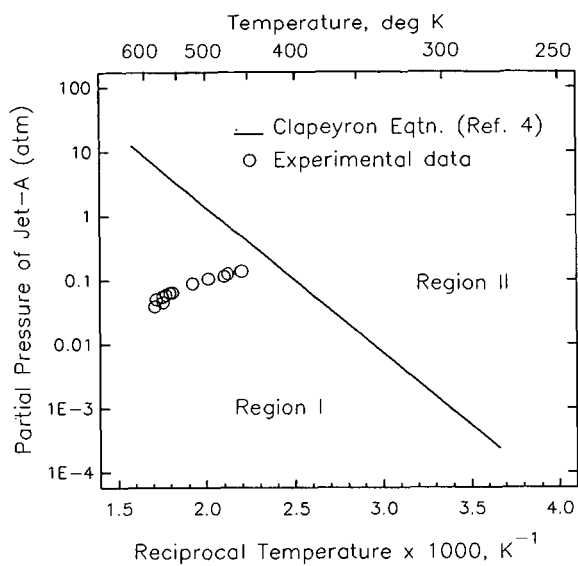


Figure 5 - Vaporization Temperature for Jet-A



INVESTIGATION OF METHODS FOR AROMATIC STRUCTURAL INFORMATION  
IN MIDDLE DISTILLATE FUELS

S.W.Lee

Energy Research Laboratories, CANMET  
Energy, Mines & Resources Canada  
555 Booth St. Ottawa. Canada. K1A 0G1

ABSTRACT

The combustion characteristics of a fuel are related to its chemical and physical properties. The fuel aromatic content is expected to have significant influence on the production of soot in the combustion process. Detailed structural information on the fuel aromatic component is desirable for prediction of soot formation and isolation of certain molecule, responsible for soot formation. Various structural parameters such as the number of aromatic rings and the extent and type of substitution could be provided by ultraviolet spectroscopy, nuclear magnetic resonance, mass spectroscopy, and supercritical fluid chromatography. Information derived from these analytical techniques for a series of middle distillate fuels will be described and relationships among the number of aromatic rings and soot formation will be discussed.

INTRODUCTION

Energy conservation technologies and energy efficiency programs are no longer new in Western world in the eighties. The global increase in demand for petroleum products and the natural decline of existing conventional crude resources reflect the industry's effort to maximize the product yield from the crude barrel and to explore suitable fossil fuel supply sources. While overall demand for distillate oils is expected to increase (1), the transportation fuels are forecast to increase in demand with the fastest rate compared to other middle distillates(2). This scenario could encourage the refiners to maximize the yield of jet fuels and diesel fuels thereby increasing the heavier components in the heating fuel pool.

In Canada, where energy demand per capita is one of the highest in the world, it is expected that, by 1995 more than half of the total domestic production will be derived from the oil sands bitumens, heavy crudes and heavy oil deposits from western Canada(3). Synthetic distillate oils processed from these nonconventional sources have entered the Canadian market over a decade and the supply is increasing. Compositional analysis of synthetic distillates showed larger proportions of aromatics with fewer proportions of paraffins compared to conventional distillates(2). Current energy conservation trends plus the use of synthetic distillate have encouraged the Canadian refiners to produce oils containing higher aromatic components. The problems associated with the use of highly aromatic fuels are widely documented and have prompted performance evaluations on various combustion equipment. At the Canadian Combustion and Carbonization Research Laboratory, a research program is being carried out to study the influence of fuel quality on burner performance in residential heating appliances.

In the course of the study, it has become apparent that reliable analytical techniques for fuel property determinations are critical for accurate interpretation of combustion performance. Especially for aromatics, a method with better accuracy and versatility than commonly used ASTM D1319(fluorescent indicator adsorption;FIA) is desirable since its detection mechanism suffers poor accuracy and its application is restricted low boiling oils only(4). The search for such a method has led to the development of a new technique utilizing supercritical fluid chromatography (5-7), and the review process of several techniques has provided relevant

information associated with each technique. In addition to total aromatic content, in depth hydrocarbon distribution data of the fuel is desirable in order to establish accurate property-performance correlations. While fuel aromatics are generally considered responsible for excessive particulate emissions, knowledge on how specific aromatic type compounds contribute to the process, could provide the lead to technologies for efficient process quality control in refinery and for reduced combustion emissions.

Initial survey of analytical data from two laboratories indicated considerable variance between a data set provided by the same method and caused concern over the accurate interpretation of results provided by different techniques. Without reliable fuel property data, accurate prediction of combustion performance can not be achieved. This document reports preliminary data from analysis of middle distillate oils, provided by five independent laboratories. Information provided by the techniques of ASTM D1319, nuclear magnetic resonance, mass spectroscopy, supercritical fluid chromatography, ultraviolet spectroscopy and silica-alumina column chromatography are described. More importantly, emphasis is given to the comparison in data supplied by independent laboratories. Correlations between soot production and specific aromatic compound types are also discussed based on the data resulted from two analysis techniques.

## EXPERIMENTAL

### Ultraviolet spectroscopy (UV)

Ultraviolet spectra of distillate samples were recorded on a UV spectrophotometer within the range of 350 nm to 190 nm after dilution with spectrograde cyclohexane solvent. 1.0, 0.10, and 0.010 cm path sample length cells were utilized with matching reference cells in the analysis depending on the aromatic concentration of the sample. Detailed analytical methodology was described elsewhere (8) and the method is currently under further refinement.

### Column chromatography

A modified procedure of the U.S. Bureau of Mines API method (9) as reported by Sawatzky et. al (10) was used to determine saturates, monoaromatics, diaromatics and polyaromatics in distillate samples. In this procedure, the saturates were eluted from the silica/alumina column with n-pentane and the aromatics with different volumetric mixtures of pentane in toluene, followed by careful removal of solvents by air drying. Dried fractions were quantified by a gravimetric method as well as a gas chromatographic method after dilution with suitable solvent.

### Supercritical fluid chromatography

The procedure for this new method for the determination of aromatics in diesel fuels and heating fuels was reported in 1987 by Fuhr et. al(5). Saturates and aromatics in distillate fuels are separated on a packed silica column (5 u silica adsorbosphere, 250mm x 2.1 mm) using supercritical carbon dioxide as mobile phase. A Shimadzu model GC-8A equipment with a flame ionization detector was used. A Varian model 8500 syringe pump was utilized to maintain the mobile phase pressure through the chromatographic column.

### Nuclear magnetic resonance spectroscopy

The  $^1\text{H}$  NMR spectra were obtained on a Varian model EM-390 spectrometer operated at 90 MHz. The samples were prepared by mixing the oil with chloroform- $\text{d}_1$  in a 50/50 volume ratio and a drop of  $\text{Me}_4\text{Si}$  was added as a reference. Total aromatic content of the fuels were calculated from hydrogen intensities by the

method of Muhl et.al (11). Aromatic breakdown compositions such as mono-,di-, poly- were further derived using other physical properties of the fuels(12).

#### Mass spectrometry

A Finnigan 4500 quadrupole mass spectrometer was used for the determination of paraffin, olefins, naphthenes, aromatics (PONA) as well as the separation of mono-, di-, and poly- aromatic fractions. The samples were separated using a 1.83m column (3% Dexil 300 on acid washed Chromosorb W) heated from 60°C to 300°C. Chemical ionization(methane) mass spectra were acquired continuously during the gas chromatographic separation on a 3 second cycle. The series of peaks characteristic of paraffins, naphthenes and aromatics were summed continuously throughout the run in characterizing the compound type classes. The olefin content was determined by the <sup>1</sup>H NMR method. The detailed PONA method is available in the published literature(13).

#### Measurement of soot production from combustion process

Soot produced in residential furnaces from the fuels are reported in terms of smoke opacity% per start cycle. It is the maximum peak opacity of the transient soot peak from a cold burner start. It represents the real life soot emission from cold temperature conditions such as in the furnace start-up in the morning after an overnight reduced thermostat setting. Opacity values also indicate general trends of other incomplete combustion products such as carbon monoxide and hydrocarbons. In addition properties of a fuel have the most significant effects on cold start operation of an appliance. The experimental program for measurement of performance characteristics in residential oil combustion has been reported elsewhere(14).

### RESULTS AND DISCUSSIONS

Two set of data from two groups of fuels are presented in this paper for discussion. One group of fuels were analyzed by four independent laboratories by NMR, MS, SFC, UV and FIA while the second group was analyzed by two laboratories using MS and column chromatography. Soot production data were available only for the second group.

In Table 1, total aromatic content as determined by four different techniques is presented. Each method determines and describes aromatics in different way. For FIA, volumetric per cent of aromatic compounds are reported whereas in MS-PONA, results are based on the fragmentation pattern and the total number of counts for each compound type. Since the total number of ion counts is proportional to weight of hydrocarbons, it can be considered as pseudo weight per cent or simply a compound type percent. SFC and NMR data are in weight per cent. The table therefore describes the type of information one can obtain from a particular method. Absolute comparison of data were not made for obvious reasons and only the correlation trends between these methods are investigated. Linear regression data are as follows.

Methods	correlation coefficient	slope of the line
SFC(wt.%) vs FIA(vol %)	0.90	0.97
SFC(wt.%) vs NMR(wt.%)	0.96	0.98
SFC(wt.%) vs MS (%)	0.92	0.81

The statistical data indicate generally good agreement between the methods with the strongest correlation between SFC and NMR. The carbon aromaticity data from Laboratory 1, from which the NMR weight per cent data are calculated is

reported in Table 2. These values represent the percentage of aromatic ring carbons present in the total numbers of carbon present in the average fuel molecule. The correlation of NMR aromaticity and SFC weight per cent show a linear relation with a correlation coefficient of 0.89 and a slope of 0.69. The aromatics by SFC are a measure of the amount of molecules having at least one aromatic ring with paraffinic and naphthenic substituents attached. Therefore this SFC-NMR correlation data with a slope of 0.69 indicates that on average, 69% of the carbon atoms in the aromatic molecules of these samples are contained in aromatic rings with the remainder in the substituents.

Table 2 also compares fuel aromaticity data provided by two independent laboratories. The data indicates that Laboratory 2 has consistently lower values than laboratory 1 for all fuels. Laboratory 2 used Brown-Ledner equation (15) whereas Laboratory 1 derived results from detailed rigorous calculations (11,12). This minor difference alone cannot be accounted for the large difference between the two laboratories. Other variables such as instrument calibration and operator manipulation techniques are more likely the cause of such discrepancy.

Table 3 contains the aromatics ring distribution information provided by NMR, UV, SFC, and MS-PONA techniques. NMR-UV pair describes ring carbon weight per cent while SFC reports aromatic breakdown in total weight per cent. Since MS data is closer to total weight per cent, it was paired with SFC data. It should be pointed out that these SFC data are resulted from preliminary experiments and additional work is being carried out currently. Monoaromatic values from each pair indicate acceptable agreement but none of the pairs show comparable values for diaromatics. Diaromatics from the UV method are significantly lower than NMR method while MS diaromatics show lower values than SFC method to a similar degree.

Table 4 reports aromatic ring distribution in other set of middle distillate fuels. Opacity % reading is the maximum soot opacity measured from a cold start transient cycle from combustion of each fuel. Limited data indicate that both monoaromatics and diaromatics from the column chromatographic method are lower than those from MS method and show no particular relation to the opacity. The column chromatographic is normally suitable for fuels having initial boiling points of at least 200°C, since light fuel components can be lost during solvent removal prior to weighing of the fractions. The method was selected for investigation based on its simplicity requiring only common laboratory equipment. The component loss during solvent removal can be eliminated by analyzing the liquid fractions by gas chromatography instead of gravimetric analysis. This would require a more complicated procedure and trained operator which offsets the simplicity of the method.

Data from column chromatographic method, monoaromatics as well as diaromatics, show no apparent trend of interrelation with soot production. Figure 1 illustrates the correlations between mono- and diaromatic fuel components determined by PONA method and opacity of soot emitted. Diaromatic compounds indicate a general relation with cold start soot emissions with the exception of few outliers. Monoaromatics do not exhibit any particular interrelation.

#### CONCLUSIONS

1. Based on the information provided by participating laboratories, NMR and SFC show the strongest agreement for total fuel aromatics weight per cent. MS data show the lowest value.
2. Fuel aromaticity determination using NMR technique by two independent laboratories resulted in significantly different values. Regardless of the technique used, the analytical results seem to be more laboratory dependent than method dependent. Due to the highly complex nature of the middle distillate, larger

discrepancies between laboratories are observed.

3. For aromatic ring distribution in fuels, no significant trends between the methods were observed. Further studies are being planned.
4. The survey of analytical techniques suggests that MS and NMR are the most powerful tools for the detailed structural information in fuel analysis. These techniques, however, are not entirely suitable to refinery process quality control.
5. It appears that supercritical fluid chromatography could be the best candidate for a new aromatic standard method for the petroleum industry. The method's agreement with NMR indicates good accuracy and it has potential application for aromatic breakdown analysis. It can handle higher boiling samples using instrumentation of moderate sophistication.
6. Preliminary studies indicates that fuel diaromatics show greater influence on soot production than monoaromatics, in residential combustion.
7. The critical requirement of a reliable analytical methods for fuel aromatic structural information still exists in combustion research.

#### ACKNOWLEDGEMENTS

The author wishes to thank Dr. B.Fuhr and Dr. C.Reichert of Alberta Research Council for their SFC work, to Dr.B.Glavincevski of National Research Council of Canada for his NMR data and Dr. L.Stavinoha of Southwest Research institute for contribution of UV data. She also wishes to express her appreciation to D.E.Barker for her technical assistance.

#### REFERENCES

1. Schrepfer, M.W., Arnold, R.J., Stansky, C.A., Oil & Gas Journal, Jan 16, 79, 1984.
2. Steere, D.E. and Nunn, T.J., SAE Technical paper series, Paper No.790922. Society of Automotive Engineers, Inc. Warrendale, PA, 1979.
3. Canadian National Energy Board, "Canadian Energy Supply and Demand 1983-2005" September 1984.
4. "Manual on Hydrocarbon Analysis", 3rd Edition, American Society for Testing and Materials, D1319. Philadelphia, PA, 1977.
5. Fuhr, B.J., Holloway, L.R., Reichert, C., and Stepler, J., Energy, Mines & Resources Canada, Energy research laboratories Contract Report No. OSQ85-00240. Ottawa, Ont, 1987.
6. Fuhr, B.J., Holloway, L.R., Reichert, C., Lee, S.W., and Hayden, A.C., American Chemical Society, Division of Fuel Chemistry preprints, 32, No.4, 30, 1987.
7. Lee, S.W., Fuhr, B.J., and Glavincevski, B., SAE Technical paper series, Paper NO. 872142, Society of Automotive Engineers, Inc. Warrendale, PA, 1987.
8. Newman, F.M. and Greenberg, M.K., U.S. Army Fuels and Lubricants Research Laboratory, Southwest Research Institute. San Antonio, TX. Government Accession No. AD A086654. Tech. Info. Centre, Caneron Station. Alexandria, VA. 1980.
9. Hirsch, D.E., Hopkins, R.L., Coleman, H.J., Cotton, F.O., and Thompson, C.J. in American Chemical Society, Div. of Petroleum Chemistry preprints. A65, 1972.
10. Sawatzky, H., George, A.E., Smiley, G., and Montgomery, D.S., Fuel, 55, 16, 1976.
11. Muhl, J., Srica, V., Mimica, B. and Tomaskovic, M., Anal. Chem., 54, 1871, 1982.
12. Glavincevski, B., private communications.
13. Ozubko, R.S., Clugston, D.M., Furimsky, E., Anal. Chem., 53, 183, 1981.
14. Lee, S.W. and Hayden, A.C., ASHRAE Transactions. 92, Part(2), American Society of Heating, Refrigeration and Air-Conditioning Engineers, Inc. Atlanta, GA, 1986.
15. Brown, J.K., and Ladner, R.W., Fuel, 39, 87, 1960.

TABLE 1. Total aromatic content of fuels as determined by different methods.

Fuel	NMR,wt.%	SFC,wt.%	FIA,vol.%	MS,%
1	41.8	40.3	35.0	28.2
2	29.1	30.7	28.9	23.4
3	30.6	34.6	41.8	19.9
4	37.1	37.1	46.7	16.4
5	43.0	42.9	37.0	25.5
6	38.2	39.1	33.3	25.1
7	33.9	30.4	25.0	19.3
8	48.2	46.8	39.1	31.2
9	57.5	55.2	63.9	29.8
10	42.3	46.4	44.7	37.2
11	87.3	80.8	74.2	68.0
12	25.2	23.8	20.6	28.6
13	29.8	28.4	24.1	16.9
14	45.9	50.2	44.9	29.5
15	48.2	49.5	43.7	31.7
16	48.7	51.7	44.2	35.7
17	61.9	69.6	64.0	46.4
18	74.6	79.0	75.0	64.7
19	30.0	37.6	33.3	21.0
20	29.9	37.6	33.0	21.0
21	29.8	37.7	24.9	20.8
22	30.3	25.4	19.6	17.9

TABLE 2. Carbon aromaticity % as determined by two different laboratories.

Fuel	NMR,% (Lab.1)	NMR,% (Lab.2)
1	28.8	20.0
2	19.1	13.0
3	20.9	14.0
4	24.1	21.0
5	29.8	24.0
6	27.2	21.0
7	21.4	14.0
8	33.5	24.0
9	35.1	28.0
10	27.0	18.0
11	59.9	50.0
12	22.4	12.0
13	15.2	12.0
14	34.6	27.0
15	33.1	25.0
16	33.7	29.0
17	47.2	42.0
18	51.9	51.0
19	14.7	16.0
20	14.6	16.0
21	19.3	16.0
22	19.6	11.0

TABLE 3. Aromatics ring distribution in fuels as determined by different methods.

Fuel	Ring carbon wt.% (NMR) vs (UV)			Aromatics wt.%(SFC)			Aromatics %(MS)					
	mono-	di-	poly-	mono-	di-	poly-	mono-	di-	poly-			
1	6.7	18.4		7.8	9.2	1.1	16.9	18.4	4.3	19.9	7.0	1.3
2	7.0	9.6		6.8	4.3	0.3	un	28.8	1.1	14.3	7.5	1.3
3	6.3	11.8		6.5	4.4	1.7	un	33.7	0.5	12.8	5.4	1.4
4	6.8	14.2		4.7	4.3	1.9	un	28.8	8.5	10.3	4.8	1.3
5	7.3	18.7		8.5	10.2	0.9	17.3	21.5	2.8	16.5	8.6	0.4
6	6.2	17.4		6.7	9.7	1.0	14.9	19.8	3.4	17.5	7.6	0.1
7	9.9	8.6		9.1	3.3	0.1	un	28.8	1.0	16.7	2.5	0.1
8	7.1	22.3		9.5	11.9	2.2	19.3	20.5	6.0	18.6	12.6	0.1
9	11.6	19.7		8.9	9.1	3.3	un	47.9	6.0	19.0	9.6	1.2
10	14.3	8.8		13.8	3.6	0.2	un	43.8	1.4	30.0	4.3	2.5
11	7.5	46.7		8.3	38.1	3.1	12.7	58.7	7.9	25.1	40.8	2.1
12	na	na		5.1	2.1	<0.1	un	22.7	na	27.2	0.9	0.5
13	na	na		9.3	2.5	<0.1	un	26.8	0.3	15.6	0.8	0.4
14	na	na		10.4	10.3	1.9	22.1	20.7	6.0	25.2	3.6	0.7
15	na	na		10.1	8.2	2.9	21.3	17.7	9.5	21.0	10.1	0.7
16	na	na		10.0	10.1	2.8	20.1	20.5	9.0	24.8	10.6	0.3
17	10.6	6.7		11.4	17.9	6.0	20.3	28.6	1.5	28.9	17.4	0.2
18	13.0	34.6		11.8	22.3	7.5	21.0	36.3	18.3	39.9	24.6	0.2
19	na	na		10.5	3.8	0.4	un	34.8	2.0	19.0	1.8	0.1
20	na	na		10.5	3.8	0.4	un	34.9	1.7	19.0	1.8	0.1
21	10.6	30.8		8.0	3.5	0.3	un	29.2	1.5	9.2	16.4	4.0
22	9.4	7.4		5.3	2.6	<0.1	un	23.9	un	16.0	1.9	<.1

na is for not available

un is for unsatisfactory separation  
value reported under di is for both mono & di

TABLE 4. Fuel aromatic ring types and their correlation to soot production.

Fuel	Aromatics Wt.% by CC			Aromatics Wt.% by MS			Smoke opacity % at cold start combustion
	mono-	di-	poly-	mono-	di-	poly	
C	18.2	16.3	1.3	29.8	11.8	0.60	1.3
D	16.2	7.2	0.2	20.7	11.5	0.83	1.2
E	14.9	7.7	0.7	18.1	6.2	0.57	1.8
F	15.9	13.6	1.9	28.9	11.5	0.99	1.5
G	31.1	31.6	1.0	41.4	38.5	0.09	31.7
L	15.9	13.4	0.3	21.3	13.0	1.03	1.9
M	23.8	23.5	0.6	43.0	19.3	2.51	52.3
N	24.5	6.3	0.4	21.5	8.4	0.31	0.7
O	55.9	22.8	0.8	30.6	43.9	1.10	16.8
P	NA			41.9	30.3	1.87	9.1
Q	13.2	6.9	0.8	41.9	30.3	1.87	1.6
S	17.4	6.6	0.9	31.5	4.2	0.12	NA
V	NA			21.6	1.8	0.27	1.6
W	NA			20.4	4.1	0.69	2.03
X	NA			28.3	15.05	0.58	2.12
Y	NA			23.5	21.65	0.71	10.45

TABLE 4. Fuel aromatic ring types and their correlation to soot production.  
(continued)

	Aromatics Wt.% by CC			Aromatics Wt.% by MS			Smoke opacity % at cold start combustion
	mono-	di-	poly-	mono-	di-	poly	
Z	NA			16.4	6.6	0.20	2.37
AA	NA			15.7	5.7	0.50	14.8
BB	NA			22.9	13.0	0.00	3.3
CC	NA			33.0	18.0	0.30	5.0
DD	NA			25.0	34.1	0.7	15.4
EE	NA			25.5	18.5	0.0	20.9
FF	NA			18.8	9.7	0.0	2.3

NA is for not available.

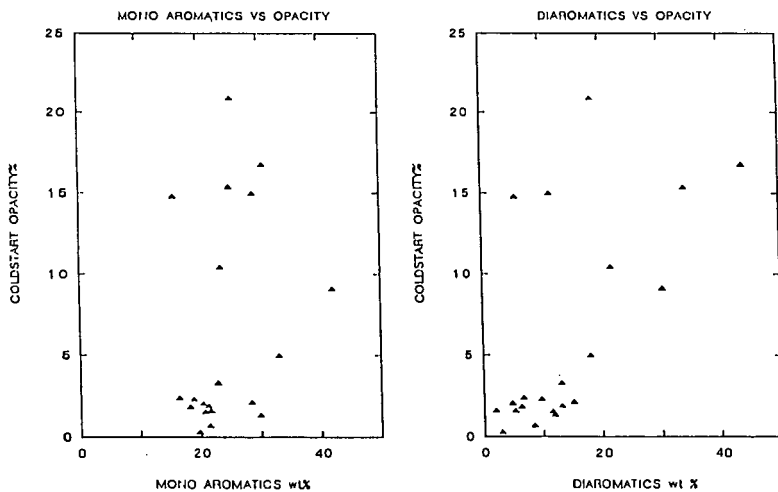


Figure 1. Correlations between fuel monoaromatic and diaromatic components and soot production at cold start combustion.

## Radiative Heating of a Conventional and Aromatic Turbine Fuel

George A. Richards

U.S. Department of Energy, Morgantown Energy Technology Center  
P.O. Box 880, Morgantown West Virginia, 26507-0880

### Introduction

Infrared radiation has long been ignored in the calculation of droplet heating rates for spray flames. Because most hydrocarbon fuels are relatively transparent to infrared radiation, it has been routine to neglect radiative heating as compared to the very effective convective heating present in high-temperature environments. Indeed, in one of the very few detailed investigations of this problem, Berlad and Hibbard (1) found that radiative heating of fuel drops was negligible compared to convection. More recent work has considered the radiative heating of water drops (2). In this case as well, the radiative heating was small when compared to convection.

However, some experimental investigations have suggested that radiation seems to improve combustion efficiency (3) as well as increase flame speeds (4). Because spray combustion is often controlled by evaporation rates, these results suggest that radiation is somehow contributing to the evaporation process. This could be potentially useful for future fuels, which may be more aromatic with lower volatility than conventional hydrocarbon fuels. For example, Myers and Lefebvre (4) found that highly aromatic fuels had flame speeds which roughly cancelled the effects of fuel volatility. They suggest that increased flame radiance via aromatic contributions to soot could heat the fuel spray and diminish the importance of fuel volatility.

While it is certain that earlier conclusions are correct concerning the relative magnitudes of radiative versus convective heating (1,2), previous studies have not considered the situation where an ambient temperature spray approaches a luminous flame. Referring to Figure 1, a room temperature spray flows toward a stationary flame, or conversely, a flame propagates through a room temperature spray. In either case, there is no convective heating of the fuel drops until the drops enter the high-temperature flame front. However, radiation has opportunity to heat the fuel spray well ahead of the flame front. Furthermore, because the drops are bathed in room temperature air, any radiative heating they experience will be rapidly transferred to the surrounding air via convection. One can thus postulate that radiation will heat not just the drops, but the air as well. The magnitude of this effect is unknown. The analysis that follows is a first effort to quantify the radiative effect.

The radiative heating problem can be divided into three subproblems:

- Radiative energy absorbed by individual drops.
- The external radiative field.
- Conservation equations for droplet and air thermal energy.

Each of these subproblems has been treated in detail, but due to space limitations, only the first will be discussed in the current work. Subsequent publications will combine results from all three analyses.

### Absorption of Radiation by a Single Drop

The absorption of radiation by small particle is covered in the texts by Van de Hulst (5) and Kerker (6). For the general problem, a laborious calculation from the Mie theory is needed to accurately compute the absorption for a single particle. However, under certain limitations, the spectral absorption cross section is given by an approximate formula:

$$Q_{\text{abs},\lambda} = 1 + 2\exp(-4sn_2)/4sn_2 + 2[\exp(-4sn_2) - 1]/(4sn_2)^2 \quad (1)$$

where

$s = \pi D/\lambda$ ; the size parameter of a particle of diameter  $D$  subject to radiation at wavelength  $\lambda$ .

$n_2 =$  the imaginary index of refraction at wavelength  $\lambda$ .

The limitations on Equation 1 are that

$$n - 1 \ll 1, \quad n_2 \ll 1 \quad (2a,b)$$

where  $n$  is the index of refraction. The restriction 2b is easily met for fuels, but the restriction 2a is not precisely met because the index of refraction for most fuels is approximately 1.3. However, for simplicity, Equation 1 will be employed here, as in other investigations. Chan and Grolmes (7) successfully utilized Equation 1 to calculate radiative heating of water drops ( $n = 1.33$ ) in a nuclear reactor cooling process. Plass (8) has compared the exact Mie solutions to Equation 1 for a range of values of  $n$ . From his results, it can be expected that Equation 1 will underestimate the absorption cross section when the restriction 2a is not met precisely. More precise evaluation can be obtained with the program due to Dave (9) or with the elegant ray-tracing procedure of Harpole (10). These complications are excluded in this initial investigation but could be easily adopted in a more comprehensive analysis.

Referring to Figure 2a, it is assumed that the spectral radiant intensity  $I_\lambda$  ( $\text{W}/\text{m}^2\text{-str-}\mu\text{m}$ ) is uniform in the  $\theta$  coordinate but has a specified intensity distribution in  $\phi$ . Note that the radiation direction is defined as positive when leaving the origin, so that the convention to define incident intensity is as shown in Figure 2b. The power absorbed by a drop of diameter  $D$  from radiation of wavelength  $\lambda$  is then

$$P_{\text{abs},\lambda} = \frac{\pi}{4} D^2 Q_{\text{abs},\lambda} \int_{4\pi} I_\lambda(\Omega) d\Omega \quad (3)$$

The integration is over the solid angle  $\Omega$ . With the assumption that  $I_\lambda$  is independent of  $\theta$  and the substitution  $\mu = \cos \phi$ , Equation 3 reduces to

$$P_{\text{abs},\lambda} = \frac{\pi}{4} D^2 Q_{\text{abs},\lambda} [2\pi \int_{-1}^1 I_\lambda(\mu) d\mu] \quad (4)$$

The term in brackets is the spectral irradiance which will be denoted  $G_\lambda$ :

$$G_\lambda = 2\pi \int_{-1}^1 I_\lambda(\mu) d\mu \quad (5)$$

Furthermore, a spectral absorption coefficient is defined for drops of diameter D:

$$C_{\text{abs},\lambda} = \frac{\pi}{4} D^2 Q_{\text{abs},\lambda} \quad (6)$$

Combining Equations 3 through 5,

$$P_{\text{abs},\lambda} = C_{\text{abs},\lambda} G_{\lambda} \quad (7)$$

Because the drop is heated by the power absorbed across the spectrum, Equation 7 must be integrated over all wavelengths to calculate the total absorbed power:

$$P_{\text{abs}} = \int_0^{\infty} P_{\text{abs},\lambda} d\lambda = \int_0^{\infty} C_{\text{abs},\lambda} G_{\lambda} d\lambda \quad (8)$$

The total irradiance G is the integral of  $G_{\lambda}$  over the spectrum:

$$G = \int_0^{\infty} G_{\lambda} d\lambda \quad (9)$$

Then Equation 8 can be written

$$P_{\text{abs}} = G \left[ \frac{\int_0^{\infty} C_{\text{abs},\lambda} G_{\lambda} d\lambda}{\int_0^{\infty} G_{\lambda} d\lambda} \right] \quad (10)$$

The expression in brackets will be denoted the total absorption coefficient for drops of diameter D:

$$C_{\text{abs}} = \frac{\int_0^{\infty} C_{\text{abs},\lambda} G_{\lambda} d\lambda}{\int_0^{\infty} G_{\lambda} d\lambda} \quad (11)$$

This reduces the expression for absorbed power to

$$P_{\text{abs}} = C_{\text{abs}} G \quad (12)$$

If the spectral nature of the incident intensity is given, then the value of  $C_{\text{abs}}$  can be computed from Equation 11. For a sooting, luminous flame, the spectral output along some direction  $\mu$  will be approximated as proportional to a blackbody at the flame temperature  $T_f$ . That is,

$$I_{\lambda}(\mu) = k(\mu) I_{\lambda b}(T_f) \quad (13)$$

Here,  $k(\mu)$  is an emissivity assumed independent of wavelength but may vary with  $\mu$ . Because the intensity  $I_{\lambda b}$  represents blackbody emission,  $k(\mu)$  is obviously restrained to values between zero and one.

Substituting Equation 13 into 11, along with the definition of  $G_{\lambda}$  from Equation 5, the total absorption coefficient is

$$C_{abs} = \frac{\int_0^{\infty} C_{abs,\lambda} (2\pi \int_{-1}^1 k(\mu) I_{\lambda b}(T_f) d\mu) d\lambda}{\int_0^{\infty} (2\pi \int_{-1}^1 k(\mu) I_{\lambda b}(T_f) d\mu) d\lambda} \quad (14)$$

Noting that  $I_{\lambda b}(T_f)$  does not depend on  $\mu$ , this reduces to

$$C_{abs} = \frac{\int_0^{\infty} C_{abs,\lambda} I_{\lambda b}(T_f) d\lambda}{\int_0^{\infty} I_{\lambda b}(T_f) d\lambda} \quad (15)$$

From Equation 12, the power absorbed by a single drop thus depends upon evaluating the droplet absorption coefficient through Equation 15 and the external irradiance  $G$ . Evaluation of Equation 14 can be completed as long as the imaginary index of refraction  $n_2$  is known (versus wavelength) for the drop medium. (Recall that  $C_{abs,\lambda}$  depends upon  $Q_{abs,\lambda}$ , Equation 6, which in turn depends upon  $n_2(\lambda)$  through Equation 1.) The value of  $n_2$  may be obtained from transmission measurements of spectral intensity incident on a liquid sample of thickness  $t$ :

$$\frac{I_{\lambda t}}{I_{\lambda i}} = \exp(-K_{\lambda} t) \quad (16)$$

where  $I_{\lambda t}$  and  $I_{\lambda i}$  denote the transmitted and incident intensity at wavelength  $\lambda$ . The absorption constant  $K_{\lambda}$  is related to the imaginary index through the following relationship (8):

$$n_2(\lambda) = K_{\lambda} \frac{\lambda}{4\pi} \quad (17)$$

Transmission measurements as in Equation 16 abound in reference manuals for spectroscopic identification (12). However, such measurements are seldom used for quantitative absorption calculations because of variations in sample thickness, spectrometer response, etc. Despite these limitations, and because no explicit data on  $n_2$  was otherwise found, spectra from several published sources will be used to calculate  $n_2$ . Published absorption spectra were corrected for window absorption by evaluating the transmission through the sample at a wavelength where the fuel was transparent. Integration is performed between 2.5 and 5.0 microns because hydrocarbons have no significant absorption bands below 2.5 microns (1) and most of the flame radiation is characterized by wavelengths shorter than 5 microns (13).

Figures 3 through 5 show the resulting calculation of  $C_{abs}$  as a function of drop size, at flame temperatures 1,200, 1,600 and 2,000<sup>abs</sup> K. Each plot provides data on the fuels toluene (highly aromatic) and JP-4. The absorption spectra of these fuels were obtained from the reference indicated on the figures, and it is interesting to note that the results for toluene were calculated with spectral data obtained in 1956 (1) and also with more recent data (1985) from reference (9). Despite different test procedures, path lengths, etc., the results are essentially the same, providing confidence that the measured spectra are sufficiently accurate for the present calculations. Further inspection of the plots reveal that the fuel type has only a modest effect on  $C_{abs}$ . The modest differences between toluene and JP-4 are of minor importance compared to the order of magnitude variations observed with changes in the drop size. For practical purposes, these results indicate that the difference in radiative adsorption properties for conventional fuels (JP-4) and aromatic fuels (toluene), is surprisingly small. As was stated at the outset, the absorption coefficient can be used to evaluate the importance of radiative heating for the propagating flame where convective heating is absent until the drops enter the flame. Because of space limitations, these calculations will be included in a subsequent publication. However, the current results can be used to verify the established notion that droplet heating is dominated by convection in back-mixed flames, i.e., practical burners. If the drops exist in an environment with air temperature  $T_{\infty} = T_f$  and black walls radiating at temperature  $T_f$ , then the ratio of convective to radiative heating is

$$\frac{\text{Radiative Heating}}{\text{Convective Heating}} = \frac{C_{abs} G}{h\pi D^2(T_f - T_s)}$$

Here,  $h$  is the convection coefficient for a sphere in a quiescent environment and may be obtained from the standard Nusselt correlation (13),  $Nu = 2$ . Considering conditions which should exaggerate the above ratio ( $T_f = 2,000^\circ K$ ,  $D = 100$  microns), the above ratio was found to be less than 0.02. The conclusion is that radiation can be ignored when droplet heating occurs by convection and radiation.

#### Summary

A simple procedure has been described to calculate a droplet absorption coefficient for infrared radiation. The coefficient can be calculated with reasonable accuracy from spectral absorption data on fuel samples. The coefficient was calculated for the fuels JP-4 and toluene. Results were relatively insensitive to fuel type but very dependent on the drop size. As expected, the results demonstrate that convection is more important than radiation in heating the drop. However, the present calculations are necessary to evaluate the radiative heating in situations where no convection operates, i.e., the propagating flame. This situation will be described in a subsequent paper.

## References

1. Berlad, A. L., and R. R. Hibbard, "Effect of Radiant Energy and Vaporization and Combustion of Liquid Fuels," NACA Research Memorandum, RM E 52 I 09 (1952).
2. Harpole, G. M., "Radiative Absorption by Evaporating Droplets," Int. J. Heat Mass Transfer, Vol. 23, pp. 17-26 (1980).
3. Nakayama, M., and T. Suzuki, "Studies on Luminous and Nonluminous Flames With Spray Combustion," Bulletin of the Japanese Society of Mechanical Engineers, Vol. 26, No. 216, June 1983.
4. Myers, G. D., and A. H. Lefebvre, "Flame Propagation in Heterogeneous Mixtures of Fuel Drops and Air," Combustion and Flame, Vol. 66, No. 2, pp. 193-210 (1986).
5. Van de Hulst, H. L., "Light Scattering by Small Particles," John Wiley and Sons (1957).
6. Kerker, M., "The Scattering of Light," Academic Press, New York (1969).
7. Chan, S. H., and M. A. Grolmes, "Hydrodynamically Controlled Rewetting," Nuclear Engineering and Design, Vol. 34, pp. 307-316 (1975).
8. Plass, G. N., "Mie Scattering and Absorption Cross Sections for Absorbing Particles," Applied Optics, Vol. 5, No. 2, pp. 279-285 (1966).
9. Dave, J. V., "Scattering of Electromagnetic Radiation by Large, Absorbing Spheres," IBM J. Res., p. 302 (1969).
10. Harpole, G. M., "Radiative Absorption by Evaporating Drops," Int. J. Heat Mass Transfer, Vol. 23, pp. 17-26 (1980).
11. Garbuny, M., "Optical Physics," Academic Press (1965).
12. Coates, J. P., and L. C. Setti, "Oils, Lubricants, and Petroleum Products: Characterization by Infrared Spectra," Marcel Decker, Inc. (1985).
13. Incropera, F., and D. Dewitt, Fundamentals of Heat Transfer, John Wiley (1981).

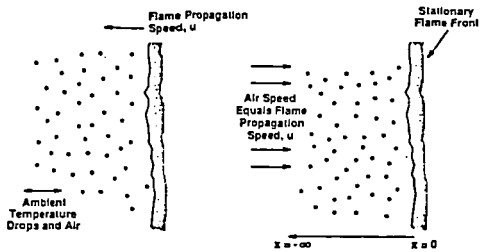


Figure 1

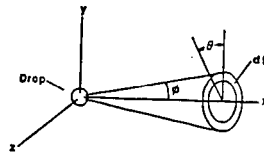


Figure 2a

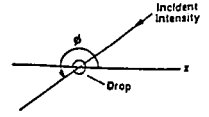


Figure 2b

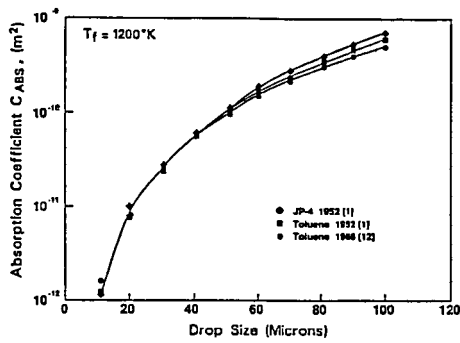


Figure 3

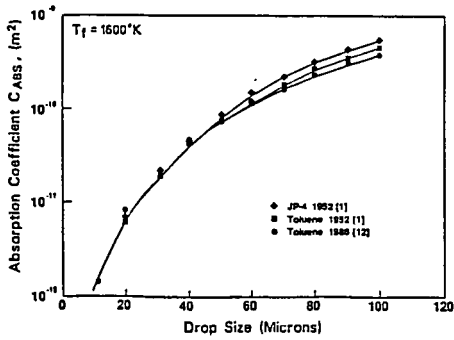


Figure 4

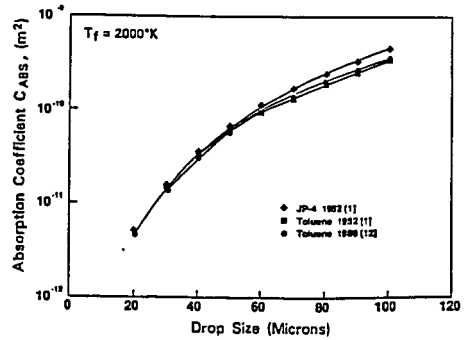


Figure 5